acapulcoites: noble gas isotopic abundances, chemical composition, cosmic-ray exposure ages, and solar cosmic ray effects. *Geochim. Cosmochim. Acta* **61**, 175–192.
Wheelock M. M., Keil K., Floss C., Taylor G. J., and Crozaz G. (1994) REE geochemistry of oldhamite-dominated clasts from the Norton County aubrite: igneous origin of oldhamite. *Geochim. Cosmochim. Acta* **58**, 449–458.
Wolf R., Ebihara M., Richter G. R., and Anders E. (1983) Aubrites and diogenites: trace element clues to their origin. *Geochim. Cosmochim. Acta* **47**, 2257–2270.
Wlotzka F. and Jarosewich E. (1977) Mineralogical and chemical compositions of silicate inclusions in the El Taco, Camp del Cielo, iron meteorite. *Smithson. Contrib. Earth Sci.* **19**, 104–125.
Yamaguchi A., Taylor G. J., Keil K., Floss C., Crozaz G., Nyquist L. E., Bogard D. D., Garrison D., Reese Y., Wiesman H., and Shih C.-Y. (2001) Post-crystallization reheating and partial melting of eucrite EET 90020 by impact into the hot crust of asteroid 4 Vesta ~4.5 Ga ago. *Geochim. Cosmochim. Acta* **65**, 3577–3599.
Yamaguchi A., Clayton R. N., Mayeda T. K., Ebihara M., Oura Y., Miura Y. N., Haramura H., Misawa K., Kojima H., and Nagao K. (2002) A new source of basaltic meteorites inferred from Northwest Africa 011. *Science* **296**, 334–336.
Yanai K. (1994) Angrite Asuka-881371: preliminary examination of a unique meteorite in the Japanese collection of Antarctic meteorites. *Proc. NIPR Symp.: Antarct. Meteorit.* **7**, 30–41.
Yanai K. and Kojima H. (1991) Yamato-74063: chondritic meteorite classified between E and H chondrite groups. *Proc. NIPR Symp.: Antarct. Meteorit.* **4**, 118–130.
Yanai K. and Kojima H. (1995) *Catalog of Antarctic Meteorites*. National Institute of Polar Research Tokyo, Japan.
Zipfel J., Palme H., Kennedy A. K., and Hutcheon I. D. (1995) Chemical composition and origin of the Acapulco meteorite. *Geochim. Cosmochim. Acta* **59**, 3607–3627.

Published by Elsevier Ltd.

*Treatise on Geochemistry*
ISBN (set): 0-08-043751-6

Volume 1; (ISBN: 0-08-044336-2); pp. 291–324

# 1.12 Iron and Stony-iron Meteorites

H. Haack
*University of Copenhagen, Denmark*
and
T. J. McCoy
*Smithsonian Institution, Washington, DC, USA*



## 1.12.1 INTRODUCTION

Without iron and stony-iron meteorites, our chances of ever sampling the deep interior of a differentiated planetary object would be next to nil. Although we live on a planet with a very substantial core, we will never be able to sample it. Fortunately, asteroid collisions provide us with a rich sampling of the deep interiors of differentiated asteroids.

Iron and stony-iron meteorites are fragments of a large number of asteroids that underwent significant geological processing in the early solar system. Parent bodies of iron and some stony-iron meteorites completed a geological evolution similar to that continuing on Earth—although on much smaller length- and time-scales—with melting of the metal and silicates, differentiation into core, mantle, and crust, and probably extensive volcanism. Iron and stony-iron meteorites are our only available analogues to materials found in the deep interiors of Earth and other terrestrial planets. This fact has been recognized since the work of Chladni (1794), who argued that stony-iron meteorites must have originated in outer space and fallen during

fireballs and that they provide our closest analogue to the material that comprises our own planet's core. This chapter deals with our current knowledge of these meteorites. How did they form? What can they tell us about the early evolution of the solar system and its solid bodies? How closely do they resemble the materials from planetary interiors? What do we know and don't we know?

Iron and stony-iron meteorites constitute ~6% of meteorite falls (Grady, 2000). Despite their scarcity among falls, iron meteorites are our only samples of ~75 of the ~135 asteroids from which meteorites originate (Keil *et al.*, 1994; Scott, 1979; Meibom and Clark, 1999; see also Chapter 1.05), suggesting that both differentiated asteroids and the geologic processes that produced them were common.

Despite the highly evolved nature of iron and stony-iron meteorites, their chemistry provides important constraints on the processes operating in the solar nebula. Although most of them probably formed through similar mechanisms, their characteristics are diverse in terms of chemistry, mineralogy, and structure. Significant differences in bulk chemistry between iron meteorites from different cores as well as variations in chemistry between meteorites from the same core provide evidence of the complex chemical evolution of these evolved meteorites. Intergroup variations for volatile siderophile elements (e.g., gallium and germanium) extend more than three orders of magnitude, hinting that iron meteorite parent bodies formed under diverse conditions. These differences reflect both the nebular source material and geological processing in the parent bodies.

Can we be sure that the iron meteorites are indeed fragments of cores? Since no differentiated asteroid has yet been visited by a spacecraft, we rely on circumstantial evidence. Some M-type asteroids have spectral characteristics expected from exposed metallic cores (Tholen, 1989), while others exhibit basaltic surfaces, a hallmark of global differentiation. Although olivine-rich mantles should dominate the volume of differentiated asteroids, there is an enigmatic lack of olivine-rich asteroids (and meteorites) that could represent mantle material (Burbine *et al.*, 1996). Until we visit an asteroid with parts of a core–mantle boundary exposed, our best evidence supporting a core origin is detailed studies of iron meteorites.

Iron–nickel alloys are expected in the cores of differentiated asteroids, but what other evidence supports the notion that iron meteorites sample the metallic cores of differentiated asteroids? What suggests that these asteroids were sufficiently heated to trigger core formation, and that iron meteorites sample cores rather than isolated pods of once molten metal? First and foremost, trace-element compositional trends in most groups of iron meteorites are consistent with fractional crystallization of a metallic melt (Scott, 1972), thus constraining peak temperatures. The temperatures required to form a metallic melt are sufficiently high to cause substantial melting of the associated silicates and trigger core formation (Taylor *et al.*, 1993). In addition, meter-sized taenite crystals and slow metallographic cooling rates in some iron meteorites suggest crystallization and cooling at considerable depth. Due to the high thermal conductivity of solid metal compared with mantle and crust materials, metal cores are believed to be virtually isothermal during cooling (Wood, 1964). Iron meteorites from the same core should therefore have identical cooling rates. Metallographic cooling rates are different from group to group but are, with the exception of group IVA, relatively uniform within each group (Mittlefehldt *et al.*, 1998). This is consistent with each group cooling in a separate core surrounded by a thermally insulating mantle.

If the iron and stony-iron meteorites came from fully differentiated asteroids, how did these asteroids heat to the point of partial melting and how did the metal segregate from the silicates? Unlike large planets, where potential energy release triggers core formation, small asteroids require an additional heat source. The heat source(s) for asteroidal melting produced a wide range of products, from unmetamorphosed chondrites to fully molten asteroids, as well as partially melted asteroids. Samples from these latter asteroids provide us with a rare opportunity to observe core formation—frozen in place.

Most iron and stony-iron meteorites came from asteroids that were sufficiently heated to completely differentiate. The better-sampled iron meteorite groups provide us with an unparalleled view of a crystallizing metallic magma. Except for an enigmatic paucity of samples representing the late stage Fe–S eutectic melt, the trends recorded by the larger groups of iron meteorites cover the entire crystallization sequence of their parent-body cores (Scott and Wasson, 1975). Within individual groups, the abundance of meteorites in each compositional range is also in good agreement with the expectations based on numerical models (Scott and Wasson, 1975).

For some asteroids, near-catastrophic impacts played an important role in their early geological evolution. Impact events ranging from local melting of the target area to complete disruption of the parent body are recorded in most groups of meteorites (Keil *et al.*, 1994). Major impacts in the early solar system caused remixing of metal and silicate and large-scale redistribution of cold and hot material in the interior of some of the parent bodies. These processes had profound consequences for the geochemical and thermal evolution of the surviving material. Later impacts on the meteorite parent bodies dispersed fragments in the solar system, some of which have fallen on the Earth in the form of meteorites. These fragments provide us with an opportunity to study the geological evolution of a complete suite of rocks from differentiated asteroids in the laboratory.



## 1.12.2 CLASSIFICATION AND CHEMICAL COMPOSITION OF IRON METEORITES

To use meteorites as a guide to parent-body evolution, we need groupings that represent individual parent bodies. In this section, we briefly discuss the characteristics of iron and stony-iron meteorites used to discriminate between the different parent bodies. Historically, iron meteorites were classified on the basis of macroscopic structure, being divided into hexahedrites, octahedrites (of varying types based on kamacite bandwidth), and ataxites (see Buchwald, 1975 and references therein). Beginning in the 1950s, it was recognized that the chemical composition of iron meteorites varied, often in concert with the structure. Today, the chemical classification—based on bulk chemical analysis of the metal—is the standard for iron meteorite groupings (see Chapter 1.05), with structural and other data (e.g., cosmic-ray exposure ages) providing supporting information about iron meteorite history.

In a series of 12 papers beginning in 1967, John Wasson and co-workers analyzed the chemistry of the vast majority iron meteorites using INAA (Wasson, 1967, 1969, 1970, 1971; Wasson and Kimberlin, 1967; Wasson *et al.*, 1989, 1998; Schaudy *et al.*, 1972; Scott *et al.*, 1973; Scott and Wasson, 1976; Kracher *et al.*, 1980; Malvin *et al.*, 1984), producing the definitive database on the chemistry and classification of iron meteorites. In the early papers, the meteorites were analyzed for nickel, iridium, gallium, and germanium, whereas the later papers include analyses for chromium, cobalt, nickel, copper, gallium, germanium, arsenic, antimony, tungsten, rhenium, iridium, platinum, and gold. Other papers by Wasson and co-workers that include analytical data have focused on individual groups or improved techniques (Scott, 1977a, 1978; Pernicka and Wasson, 1987; Rasmussen *et al.*, 1984; Wasson and Wang, 1986; Choi *et al.*, 1995; Wasson, 1999; Wasson and Richardson, 2001). Additional resources on the chemical composition of iron meteorites include Buchwald (1975), Moore *et al.* (1969) (nickel, cobalt, phosphorus, carbon, sulfur, and copper), and Hoashi *et al.* (1990, 1992, 1993a,b) (platinum group elements).

Although the original classification was entirely based on chemistry, additional data on structure, cooling rates, and mineralogy suggest that it is a genetic classification where each group represents one parent core (Scott and Wasson, 1975). The chemical compositions within each group form coherent trends generally consistent with fractional crystallization and the members have similar or uniformly varying structure and mineralogy. Despite significant overlap in the compositional clusters, multiple elements, along with structure and mineralogy, distinguish the groups. Most groups have uniform cooling rates, supporting the idea that each group represents an individual asteroid core. Cosmic-ray exposure ages further support a genetic classification in groups IIIAB and IVA, where most members have cosmic-ray exposure ages of 650 Ma and 400 Ma, respectively.

A detailed description of the individual iron meteorite groups is found in Scott and Wasson (1975). We include a brief synopsis of some of the important characteristics of the largest groups, particularly those with implications for the evolution of the parent bodies. Differences between these groups serve to illustrate some of the diverse characteristic of iron meteorites. The groups range from the volatile and silicate-rich IAB–IIICDs to the highly volatile depleted groups IVA and, in particular, IVB. Differences in the oxygen fugacities of the parent cores are reflected in the difference in mineralogy between the highly reduced IIABs and the more oxidized group IIIAB iron meteorites.

### 1.12.2.1 Group IIAB Iron Meteorites

Group IIAB iron meteorites (103 members) have the lowest nickel concentrations of any group of iron meteorites (5.3–6.6 wt.% Ni) (see figure 26, Chapter 1.05). The IIAB irons exhibit a distinct structural appearance, owing to their low bulk nickel concentration and, thus, predominance of kamacite. Structurally, they range from hexahedrites (former group IIA) to coarsest octahedrites (former group IIB). In hexahedrites, kamacite crystals are generally larger than the specimen, whereas coarsest octahedrites have kamacite lamellae wider than 3.3 mm (Buchwald, 1975). The low nickel concentration, absence of phosphates (Buchwald, 1975, 1984), and occurrence of graphite in IIAB iron meteorites suggest formation from highly reduced material.

### 1.12.2.2 Group IIIAB Iron Meteorites

With 230 classified meteorites, IIIAB is by far the largest group of iron meteorites. IIIAB irons are medium octahedrites, often heavily shocked

(Buchwald, 1975; Stöffler *et al.*, 1988), and have uniform exposure ages and cooling rates. They have the by far highest abundance of phosphates, suggesting formation from relatively oxidized material (Kracher *et al.*, 1977; Olsen and Fredriksson, 1966; Olsen *et al.*, 1999). Silicate inclusions are documented in only two members (Haack and Scott, 1993; Kracher *et al.*, 1977; Olsen *et al.*, 1996). Observed compositional trends can be broadly matched by numerical models for fractional crystallization of a common core (Haack and Scott, 1993; Ulff-Møller, 1998; Chabot and Drake, 1999; Wasson, 1999; Chabot and Drake, 2000). Metallographic cooling rates of IIIAB iron meteorites are fairly uniform with an average of 50 K $Myr^{-1}$ (Rasmussen, 1989), corresponding to a parent-body diameter of ~50 km (Haack *et al.*, 1990). An interesting feature of IIIAB's is that 19 of 20 measured cosmic-ray exposure ages point to a breakup of the parent core 650 ± 100 Myr ago (Voshage, 1967; Voshage and Feldmann, 1979; see Chapter 1.13), suggesting catastrophic dispersal then (Keil *et al.*, 1994). The large number of IIIAB iron meteorites and the almost complete absence of unusual or poorly understood features make group IIIAB iron meteorites the best available samples of a crystallized metal core from a differentiated body.

#### 1.12.2.3 Group IVA Iron Meteorites

IVA irons are fine octahedrites (Buchwald, 1975). With 48 members, IVA is the third-largest group. They have very low volatile concentrations and an unusually low Ir/Au ratio. The chemical trends defined by group IVA are broadly consistent with numerical models of fractional crystallization (Scott *et al.*, 1996; Wasson and Richardson, 2001). Several features of group IVA suggest a complex parent body evolution after core crystallization. Two IVA irons contain rare tridymite crystals and two others contain ~50 vol.% silicates mixed with metal on a centimeter scale (Haack *et al.*, 1996a; Reid *et al.*, 1974; Scott *et al.*, 1996; Ulff-Møller *et al.*, 1995). Although the metal in the latter two crystallized within the solid silicate matrix, it has normal structure, chemistry, and cooling rate for group IVA (Schaudy *et al.*, 1972; Haack *et al.*, 1996a; Scott *et al.*, 1996). Metallographic cooling rates of group IVA irons are the subject of dispute between those who believe that an apparent cooling rate variation correlated with nickel concentration is an artifact (Willis and Wasson, 1978a,b; Wasson and Richardson, 2001) and those that favor a true variation (Moren and Goldstein, 1978, 1979; Rasmussen, 1982; Rasmussen *et al.*, 1995; Haack *et al.*, 1996a). Haack *et al.* (1996a) argued that the diverse, but slow, metallographic cooling rates and evidence of rapid cooling from 1,200 °C of the tridymite–pyroxene assemblage in one of the stony-irons, Steinbach, implied that the IVA parent body went through a breakup and reassembly event shortly after core crystallization. The model was disputed by Wasson and Richardson (2001), who argued that the apparent correlation between metallographic cooling rates and chemistry for IVA iron meteorites implies that the cooling rates are in error. Like IIIAB, they are often heavily shocked and have similar cosmic-ray exposure ages of ~400 ± 100 Ma (Voshage, 1967; Voshage and Feldmann, 1979; see Chapter 1.13) suggesting parent-body disruption at that time (Keil *et al.*, 1994). A recent compilation of the chemical compositions of IVA iron meteorites may be found in Wasson and Richardson (2001).

#### 1.12.2.4 Group IVB Iron Meteorites

Despite containing only 13 members, group IVB exhibits unique properties and deserves special mention. Group IVB irons have the lowest volatile concentrations of any group (Table 1; see figure 26, Chapter 1.05). IVB is also enriched in refractory elements, with iridium, rhenium, and osmium concentrations an order of magnitude higher than in any other group of irons (Scott, 1972; see also Table 1). No chondrite groups have siderophile compositions similar to group IVB iron meteorites (Rasmussen *et al.*, 1984). Re–Os systematics (Smoliar *et al.*, 1996) suggest that IVB irons, unlike other groups, require a nonchondritic osmium reservoir. High metallographic cooling rates of IVB irons (Rasmussen *et al.*, 1984) suggest a small parent body.

**Table 1** Average compositions of meteorites from the major iron and stony-iron meteorite groups.

| Group | *Re* (ng $g^{-1}$) | *Ir* (μg $g^{-1}$) | *Ni* (wt.%) | *Co* (mg $g^{-1}$) | *Cu* (μg $g^{-1}$) | *Au* (μg $g^{-1}$) | *Ga* (μg $g^{-1}$) | *Ge* (μg $g^{-1}$) | *S* (wt.%) | |
|---|---|---|---|---|---|---|---|---|---|---|
| IAB | 260 | 2.0 | 9.50 | 4.9 | 234 | 1.75 | 63.6 | 247 | | |
| IIAB | 1,780 (250) | 12.5 (1.3) | 5.65 | 4.6 | 133 | 0.71 (1.0) | 58.63 | 174 | (17) | |
| IIIAB | 439 (200) | 3.2 (5.0) | 8.33 | 5.1 | 156 | 1.12 (0.7) | 19.79 | 39.1 | (12) | |
| IVA | 230 (150) | 1.8 (1.8) | 8.51 | 4.0 | 137 | 1.55 (1.6) | 2.14 | 0.12 | (3) | |
| IVB | 2,150 (3,500) | 18.0 (22) | 17.13 | 7.6 | <9 | 0.14 (0.15) | 0.23 | 0.055 | (0) | |

Data are from the references listed in Section 1.12.2. Numbers in parentheses are the calculated initial liquid compositions of the core from Chabot and Drake (2000) (Re, S) and Jones and Drake (1983) (Ir, Au). Note the significant differences between the estimates of the initial liquid and the average meteorite compositions. For elements such as Re and Ir with distribution coefficients between solid and liquid metal that are far from unity, the average meteorite composition may be different from the initial composition of the liquid core (see also table 3, Mittlefehldt *et al.*, 1998).



#### 1.12.2.5 Silicate-bearing Iron Meteorites

Group IAB, IIICD, and IIE irons differ in a number of properties from other iron groups. The compositional trends in these groups are unlike those in other irons (e.g., IIIAB) for which an origin by fractional crystallization of a common metallic core is inferred. Although sometimes termed "nonmagmatic," IAB, IIICD, and IIE irons clearly experienced melting during their history, although perhaps of a different type than, for example, group IIIAB. Unlike other groups, metals in IAB and IIICD irons show considerable ranges in nickel, gallium, and germanium concentrations but very restricted ranges for all other elements (see figure 26, Chapter 1.05). Iridium in these groups varies within a factor of 10, compared to more than three orders of magnitude in IIIAB. These trends cannot be explained by simple fractional crystallization (Scott, 1972; Scott and Wasson, 1975). IAB irons also have metal compositions close to cosmic abundances (Scott, 1972), suggesting limited parent-body processing.

Silicates provide further evidence for the unusual origin of IAB–IIICD. While differentiated silicates might be expected in association with iron meteorites, silicates in IAB–IIICD irons are broadly chondritic (Mittlefehldt *et al.*, 1998; Benedix *et al.*, 2000; see Chapter 1.11). Models for the origins of IAB–IIICD iron meteorites include crystallization of a sulfur- and carbon-rich core in a partially differentiated object (Kracher, 1985; McCoy *et al.*, 1993), breakup and reassembly of a partially differentiated object at its peak temperature (Benedix *et al.*, 2000), or crystal segregation in isolated impact melt pools on the surface of a porous chondritic body (Wasson and Kallemeyn, 2002). A recent compilation of the chemical compositions of IAB and IIICD iron meteorites may be found in Wasson and Kallemeyn (2002).

Group IIE is a much smaller group with very diverse characteristics in terms of metal textures and silicate mineralogy. The chemical composition of the metal is very restricted and inconsistent with fractional crystallization (Scott and Wasson, 1975; Wasson and Wang, 1986). The silicate inclusions range from metamorphosed chondrites (e.g., Netschaevo) to highly differentiated silicates (e.g., Kodaikanal, Weekeroo Station), with intermediate members present (e.g., Watson, Techado) (Bogard *et al.*, 2000). The most primitive members of the group resemble H chondrites in both mineral chemistry and oxygen isotopic composition (Clayton and Mayeda, 1996; Ruzicka *et al.*, 1999), although the match is not perfect (Bogard *et al.*, 2000). The most perplexing feature of this group is the presence of silicate inclusions which give chronometric ages of ~3.8 Ga, suggesting formation ~0.8 Ga after the formation of the solar system. A range of models have been proposed in the past decade, including both impact-induced (Olsen *et al.*, 1994; Ruzicka *et al.*, 1999) and incipient parent-body melting (Bogard *et al.*, 2000). Young chronometric ages would virtually require that impact played a role in the formation of some members of this group.

#### 1.12.2.6 Mesosiderites

Mesosiderites are arguably the most enigmatic group of differentiated meteorites. Mesosiderites are breccias composed of roughly equal proportions of Fe–Ni metal and silicates. Unlike pallasites, where the silicates are consistent with a deep mantle origin, the silicates in the mesosiderites are basaltic, gabbroic, and pyroxenitic (Powell, 1971; see Chapter 1.11). Metal compositions of mesosiderites are almost uniform, suggesting that the metal was molten when mixed with the silicates (Hassanzadeh *et al.*, 1989). Many innovative models have attempted to explain the enigmatic mixture of crustal materials with core metal (see review in Hewins, 1983). Some relatively new models include impacts of molten planetesimals onto the surface of a large differentiated asteroid (Rubin and Mittlefehldt, 1992; Wasson and Rubin, 1985) and breakup and reassembly of a large differentiated asteroid with a still molten core (Scott *et al.*, 2001).

Another unusual characteristic of mesosiderites is their very slow metallographic cooling rates of less than 1 K $Myr^{-1}$ (Powell, 1969; Haack *et al.*, 1996b; Hopfe and Goldstein, 2001). These cooling rates are the slowest for any natural geological material, suggesting that the mesosiderite parent body must have been large. Mesosiderites have young Ar–Ar ages of ~3.95 Ga (Bogard and Garrison, 1998). The young Ar–Ar ages have been attributed to extended cooling within a large asteroid (Haack *et al.*, 1996b; Bogard and Garrison, 1998) or impact resetting (Bogard *et al.*, 1990; Rubin and Mittlefehldt, 1992).

#### 1.12.2.7 Ungrouped Iron Meteorites

Iron meteorites require a large number of parent bodies to account for their diverse properties. Ungrouped irons alone require 40–50 different parent bodies (Scott, 1979; Wasson, 1990), a number unmatched by the types of meteorites that represent mantle and crust materials (Burbine *et al.*, 1996). In addition, gallium and germanium

concentrations of ungrouped irons are not randomly distributed as expected if they represent a large and continuous population of poorly sampled parent bodies (Scott, 1979). Ungrouped irons tend to have gallium and germanium concentrations in the same ranges as those defined by the original Ga–Ge groups I–IV. The origin of ungrouped irons is poorly understood. While many of them sample poorly known asteroidal cores, they include a variety of anomalous types, including highly reduced silicon-bearing irons (e.g., Horse Creek) and at least one that essentially quenched from a molten state (e.g., Nedagolla).

### 1.12.3 ACCRETION AND DIFFERENCES IN BULK CHEMISTRY BETWEEN GROUPS OF IRON METEORITES

The most striking differences in chemical composition between groups of iron meteorites are the differences in concentration of volatile elements (several orders of magnitude) and the smaller but important threefold variation in nickel concentration (Table 1). These bulk chemical differences cannot be attributed to fractional crystallization of asteroidal cores (Scott, 1972), but suggest that processes during asteroid accretion and core-formation produced metallic melt bodies with a range of compositions. These processes occurred exclusively in the nebula (condensation–evaporation), in both nebular and parent-body settings (oxidation–reduction) and exclusively on the parent body (metal–silicate segregation, degassing of volatiles and impacts). In some cases, it is possible to relate specific chemical characteristics of an iron meteorite group to a specific process, but in most cases some ambiguity remains. In this section, we discuss the diverse chemical compositions of iron meteorites and its possible origins.

Chondrites are generally considered representative of the material from which asteroids, including iron meteorite parent bodies, and planets formed. The heterogeneity of primitive chondrites shows that solids in the early solar system were, to some extent, chemically and isotopically diverse. Metal abundances range from zero in some carbonaceous chondrites (e.g., CI and CM) to more than 60 wt.% in some CH/CB chondrites (Campbell *et al.*, 2001; see Chapter 1.05). The chemical composition of chondritic metal is also diverse, primarily reflecting oxidation–reduction processes, although in rare cases the metal formed as high temperature condensates (Kong and Ebihara, 1997; Kong *et al.*, 1997; Campbell *et al.*, 2001). Although ordinary chondrites are depleted in gallium and germanium by up to an order of magnitude relative to CI chondrites (Wasson and Wai, 1976), the variation in volatile concentrations observed among iron meteorite groups has no counterpart in chondrites.

The main processes that control the composition of nebular metal—condensation and fractionation from the gas at high temperatures and oxidation–reduction processes (Kelly and Larimer, 1977)—are illustrated in Figure 1. Oxidation of iron from the metal will enrich the remaining metal in elements less easily oxidized than iron. Differences in mineralogy and chemistry between iron meteorite groups show that oxidation–reduction processes were important. The oxygen fugacity of the molten core is reflected in the abundance of the oxygen-bearing phosphates found in some groups of iron meteorites (Olsen and Fredriksson, 1966; Olsen *et al.*, 1999). Phosphate minerals are typical in group IIIAB but have never been observed in IIAB iron meteorites (Buchwald, 1975, 1984; Scott and Wasson, 1975). The higher nickel concentration in group IIIAB compared to IIAB (Table 1) is consistent with the latter forming from more reduced material. Whether this difference is a result of a nebula process or a parent-body process remains an open question.

The other important process in the nebula is condensation and fractionation from the gas. Condensation at high-temperatures results in refractory element enrichment and volatile depletion. High-temperature condensates may be preserved if isolated from the gas before more volatile elements condense (Meibom *et al.*, 2000; Petaev *et al.*, 2001). Processes operating within the parent bodies may mask this process. Volatile-element depletions could result from degassing of the parent-body during heating, partial melting, and impact (Rasmussen *et al.*, 1984; Keil and Wilson, 1993). Parent-body degassing will not, however, result in significant refractory element enrichment. Thus, it may be possible to distinguish volatile depletions caused by high-temperature condensation and parent-body degassing.

The best evidence for the importance of condensation and fractionation is the composition of group IVB irons and ungrouped irons of similar composition (Figure 2). The bulk compositions of groups IVA and IVB irons are consistent with high-temperature condensation of the source material (Kelly and Larimer, 1977) (Figure 1). These groups are depleted in the volatile to moderately volatile elements sulfur, phosphorus, gallium, germanium, phosphorus, antimony, copper, and gold, with the nonmetals sulfur and phosphorus of particular importance, since they have significant effects on core crystallization and Widmanstätten pattern formation. While the depletion of volatile elements in group IVA can result from parent-body degassing (Keil and Wilson, 1993), enrichments in the refractory



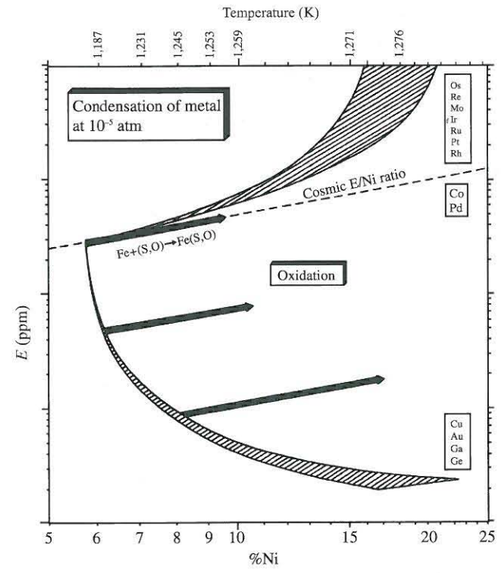


**Figure 1** Compositional evolution of metal condensing at a pressure of $10^{-5}$ atm. The first metal to condense contains 19 ± 3 wt.% Ni and decreases to the cosmic value of 5.7 wt.% Ni as cooling commences. Elements more refractory than Ni are enriched in the early condensates, whereas elements more volatile than Ni are depleted. Oxidation of Fe shifts the composition of the metal in the direction of the heavy arrows (Kelly and Larimer, 1977) (reproduced by permission of Elsevier from *Geochim. Cosmochim. Acta*, **1977**, *41*, 93–111).

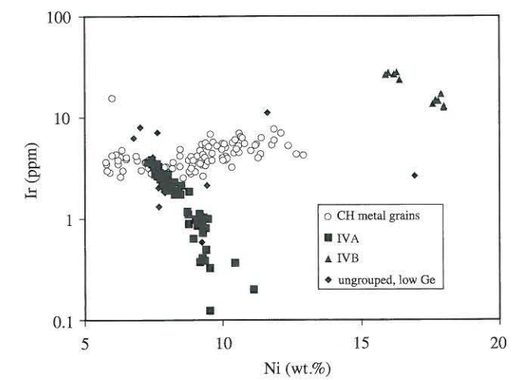


**Figure 2** Ni versus Ir for group IVA and IVB iron meteorites and a number of ungrouped iron meteorites with low Ge concentrations and compositions intermediate between IVA and IVB. Also shown are compositions of zoned metal grains from CH-like chondrites (sources Campbell *et al.*, 2001; Wasson and Richardson, 2001; Rasmussen *et al.*, 1984).

elements rhenium, osmium, and iridium in group IVB cannot (Kelly and Larimer, 1977; Scott, 1972; Wasson and Wai, 1976). High-temperature condensation for group IVA might also explain the unusually high nickel concentration, although oxidation cannot be excluded (Figure 1).

The source material for IVB irons is not preserved among known chondrites (Rasmussen *et al.*, 1984), although a few CB chondrites contain metal grains thought to sample high-temperature condensates (Meibom *et al.*, 2000; Campbell *et al.*, 2001; see Chapter 1.05). These metal grains are compositionally intermediate between IVA and IVB irons (Figure 2) and may be the first direct evidence that such materials were produced in the nebula. A close relationship

between type IVA and IVB irons and CB chondrites is also suggested by the elevated $\delta^{15}N$ values in all three groups (Kerridge, 1985; Prombo and Clayton, 1985, 1993). Metal from IVB irons would have been isolated from a nebular gas above 1,500 K (Petaev *et al.*, 2001), even higher than metal grains in CB chondrites. The postulated chondritic metal corresponding to IVB irons was either entirely incorporated into bodies that differentiated, or these chondrites remained unsampled.

### 1.12.4 HEATING AND DIFFERENTIATION

How did asteroidal cores come to exist in the first place? What were the physical processes? What were the heat sources? In this section, we address these fundamental issues by considering evidence from iron meteorites, primitive chondrites, achondrites, experiments, and numerical calculations. The simplest case for core formation is metal sinking through a silicate matrix that has experienced a high degree of partial melting. Numerous experimental studies (e.g., Takahashi, 1983; Walker and Agee, 1988; McCoy *et al.*, 1998) demonstrate that metal and sulfide tend to form rounded globules, rather than an interconnected network, at moderate degrees of silicate partial melt. These globules then sink through silicate mush. Taylor (1992) calculated that at silicate fractions of 0.5, metal particles ~10–1,000 cm sink readily through a crystal mush, although it remains unclear how millimeter-sized metal particles in primitive chondritic meteorites attain these sizes. Settling would be rapid, with core formation requiring tens to thousands of years, depending on parent-body size and degree of silicate melting. Many large iron meteorites (e.g., Canyon Diablo, Hoba) and shower-producing irons (e.g., Gibeon) exceeded 1–10 m, supporting the idea that irons originated in central cores, rather than dispersed metallic masses.

A more interesting case is porous flow through interconnected networks in a largely solid silicate matrix. This scenario is of interest both because any fully melted body would have experienced an earlier stage of partial melting and because early partial melts are sulfur enriched. The Fe, Ni–FeS eutectic occurs at ~950 °C and contains ~85 wt.% FeS (Kullerud, 1963). Using Darcy's law, Taylor (1992) calculated flow velocities of 270 m $yr^{-1}$ at 10% melting, suggesting core formation ~$10^2$–$10^4$ yr. Taylor (1992) did note considerable uncertainty about interfacial angles, which control melt migration, in Fe,Ni–FeS melts and that considerable experimental evidence argued against metal-sulfide melt migration at low degrees of partial melting under static conditions. In contrast, Urakawa *et al.* (1987) suggested that oxygen-rich melts at higher pressure might readily segregate. Rushmer *et al.* (2000) reviewed recent experimental evidence for metal-sulfide melt migration at pressures from 1 atm to 25 GPa (Herpfer and Larimer, 1993; Ballhaus and Ellis, 1996; Minarik *et al.*, 1996; Shannon and Agee, 1996, 1998; Gaetani and Grove, 1999). For our purposes, many of these experiments are limited in their utility, since pressures in even the largest asteroids were only fractions of a GPa (Rushmer *et al.*, 2000). These experiments demonstrate that only anion-dominated metallic melts exhibit dihedral angles less than 60° and form interconnected networks (Figure 3). This is consistent with the work of Taylor (1992) and suggests that even Fe–S eutectic melts at low pressure (anions/cations ~0.8) would not migrate to form a core under static conditions.

Perhaps dynamic processes played a role in the formation of asteroidal cores. Rushmer *et al.* (2000) found considerable evidence for iron sulfide melt mobility in the absence of silicate partial melting in experiments on an H6 ordinary chondrite. These authors suggest that metal-sulfide segregation may be possible, although the pressure–strain regime used may not be applicable to asteroidal-sized bodies. Keil and Wilson (1993) suggested that overpressure during Fe,Ni–FeS eutectic melting might create veins and volatiles might cause these veins to rise in small bodies.

These results suggest two very different types of cores result from partial melting. At low degrees of partial melting, cores may be sulfur-rich or even

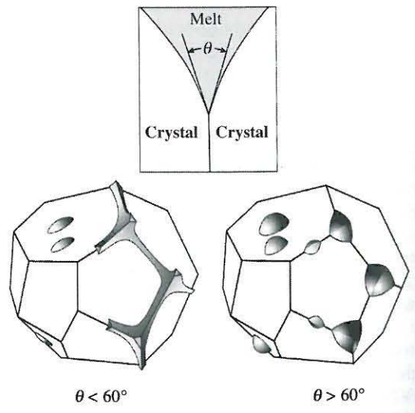


**Figure 3** Illustration of the dihedral angle $\theta$ and a depiction of two end-member microstructures for static systems. If $\theta < 60°$, an interconnected network will form and melt migration can occur. If $\theta > 60°$, melt forms isolated pockets. In experimental systems, interconnectedness only occurs in anion-rich static systems.



sulfur-dominated. The small sulfur rich cores would coexist with a mantle that contains essentially chondritic silicate mineralogy and metal abundance. As near-total melting is achieved, metal drains efficiently to the center of the body, forming metal-dominated cores, which may be depleted in sulfur relative to the chondritic precursor as a result of explosive removal of the Fe,Ni–FeS eutectic melt (Keil and Wilson, 1993).

While most meteorites sample either primitive or fully differentiated asteroids, a few offer direct evidence for processes occurring during core formation. Acapulcoites and lodranites (McCoy *et al.*, 1996, 1997a, b; Mittlefehldt *et al.*, 1996) offer tantalizing clues to the nature of asteroidal core formation. In the acapulcoites, millimeter- to centimeter-long veins of Fe,Ni–FeS eutectic melts formed in the absence of silicate partial melting (Figure 4). The bulk composition of these samples is unchanged from chondritic, suggesting that only localized melt migration occurs. In contrast, lodranites are depleted in both plagioclase–pyroxene (basaltic) melts and the Fe,Ni–FeS eutectic melts, suggesting that silicate partial melting opened conduits for metal-sulfide melt migration. While sulfur-rich cores may have formed at low degrees of partial melting (e.g., <20%), they required silicate partial melting. Impact during core formation is a complicating factor. Mesosiderites and silicate-bearing IAB and IIICD irons may have formed by disruption of a partially to fully differentiated parent body prior to core crystallization and solidification (Benedix *et al.*, 2000; Scott *et al.*, 2001). The consequences of an impact during core formation/crystallization have not been fully explored.

Iron meteorite parent bodies experienced heating and melting at temperatures in excess of 1,500 °C (Taylor, 1992). What was the heat source? Melting occurred very early in solar system history. $^{182}Hf$–$^{182}W$ and $^{187}Re$–$^{187}Os$ systematics in iron meteorites (e.g., Horan *et al.*, 1998) suggest core formation within 5 Myr of each other and formation of the first solids in the solar system. Early differentiation is also supported by the presence of excess $^{26}Mg$ from the decay of extinct $^{26}Al$ (half-life of 0.73 Ma) in the eucrites Piplia Kalan (Srinivasan *et al.*, 1999) and Asuka-881394 (Nyquist *et al.*, 2001).

**Figure 4** The Monument Draw acapulcoite contains centimeter scale veins of Fe,Ni metal and troilite formed during the first melting of asteroids. In the absence of silicate melting, these veins were unable to migrate substantial distances and, thus, would not have contributed to core formation. Length of specimen is ~7.5 cm (Smithsonian specimen USNM 7050).

Several heat sources for core formation can be ruled out. Early melting was not caused by decay of the long-lived radionuclides (e.g., uranium, potassium, and thorium) that contribute to the Earth's heat budget. Similarly, accretional heating—which could have caused planet-wide melting in the terrestrial planets—would have produced heating of no more than a few tens of degrees in asteroids. Keil *et al.* (1997) argued that the maximum energy released during accretion is equal to the gravitational binding energy of the asteroid after accretion. For a 100 km body, this equates to a temperature increase of only 6 °C. Finally, impacts sufficiently energetic to melt asteroids will also catastrophically disrupt the asteroid.

The most likely heat sources for melting of asteroidal parent bodies are electrical conduction heating by the T-Tauri solar wind from the pre-main-sequence Sun (e.g., Sonett *et al.*, 1970) or short-lived radioactive isotopes (Keil, 2000). Melting of asteroids by $^{26}Al$ has gained broader acceptance since the discovery of excess $^{26}Mg$ in Piplia Kalan (Srinivasan *et al.*, 1999). Taylor (1992) points out an interesting conundrum. In chondrites, $^{26}Al$ is concentrated in plagioclase—an early melting silicate. Loss of basaltic melts leaves plagioclase- and troilite-depleted residues akin to the lodranites (e.g., McCoy *et al.*, 1997a), which are sufficiently depleted in $^{26}Al$ that no further heating occurs. Several authors (e.g., Shukolyukov and Lugmair, 1992) suggest $^{60}Fe$ as a heat source. Recent evidence for very high concentrations of $^{60}Fe$ in chondritic troilite (Mostefaoui *et al.*, 2003; Tachibana and Huss, 2003) raises the possibility that $^{60}Fe$ could cause melting even in the absence of other heat sources. Occurring in both oxidized and reduced forms, $^{60}Fe$ would be retained throughout all layers of a body during differentiation and could provide the heat necessary for global melting and, ultimately, core formation in asteroids.

### 1.12.5 FRACTIONAL CRYSTALLIZATION OF METAL CORES

Although iron meteorites provide a guide to understanding the ongoing crystallization of the Earth's core, important differences in the physical

settings exist. First and foremost, the central pressures within the iron meteorite parent bodies did not exceed 0.1 GPa, compared to central pressures in excess of 350 GPa on Earth. The steep pressure gradient in the Earth's core, which causes the core to crystallize from the inside out, was absent in the asteroidal cores. Since the core is cooled through the mantle, Haack and Scott (1992) argued that the onset of core crystallization in asteroids was probably from the base of the mantle. Crystallization of the asteroidal cores was likely in the form of kilometer-sized dendrites as light buoyant liquid, enriched in the incompatible element sulfur inhibited crystallization of the outer core.

The fractional crystallization trends preserved in iron meteorites are unparalleled in terrestrial magmatic systems. Trace-element variations span more than three orders of magnitude within group IIIAB irons (Figure 5). The traditional way to display the bulk compositional data of iron meteorites is in a log nickel versus log element diagram. More recent work has used gold as the reference element (Wasson, 1999; Wasson and Richardson, 2001). Gold is a better choice because the distribution coefficient is further from unity giving a natural variation that far exceeds the analytical uncertainty (Haack and Scott, 1993). In a log $E$ versus log Ni diagram, ideal fractional crystallization from a perfectly mixed liquid with constant distribution coefficients will result in straight chemical trends where the slope is given by $(D_E - 1)/(D_{Ni} - 1)$, where $D_E$ and $D_{Ni}$ are the liquid metal/solid metal distribution coefficients for the element and nickel, respectively. Although most trends define almost straight lines, differences in slope from group to group and curved trends for some elements such as gallium and germanium show that the distribution coefficients cannot be constant. The slopes of the Ni–Ir trends correlate with the volatile concentrations (including sulfur) for the different groups. Experimental work has shown that the distribution coefficients are functions of the phosphorus, sulfur, and carbon concentration in the liquid (Goldstein and Friel, 1978; Narayan and Goldstein, 1981, 1982; Willis and Goldstein, 1982; Jones and Drake, 1983; Malvin *et al.*, 1986; Jones and Malvin, 1990; Chabot and Drake, 1997, 1999, 2000; Liu and Fleet, 2001; Chabot and Jones, 2003). Using the experimentally determined distribution coefficients it is possible to calculate fractional crystallization trends (Figure 5). Early numerical models assumed that the liquid remained perfectly mixed throughout crystallization (Willis and Goldstein, 1982; Jones and Drake, 1983), whereas later models have included the effects

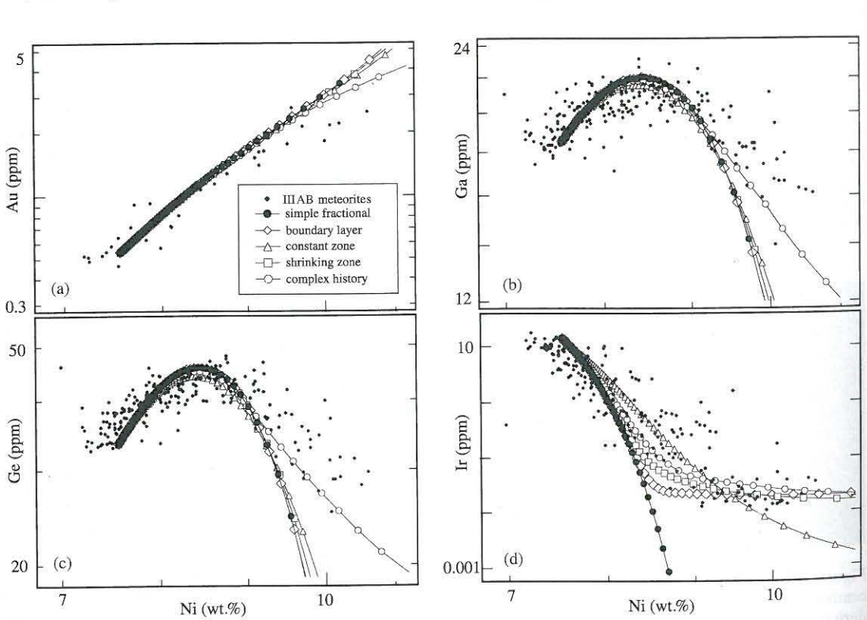


**Figure 5** Calculated fractional crystallization trends for group IIIAB iron meteorites using several different types of models. The simple fractional crystallization models assume a perfectly mixed liquid whereas the other four models assume different types of imperfect mixing (reproduced by permission of the Meteoritical Society from *Meteorit. Planet. Sci.* **1999**, *34*, 235–246).



of assimilation (Malvin, 1988), imperfect mixing of the liquid (Chabot and Drake, 1999), liquid immiscibility (Ulff-Møller, 1998; Chabot and Drake, 2000), and trapping of sulfur-rich liquid (Haack and Scott, 1993; Scott *et al.*, 1996; Wasson, 1999; Wasson and Richardson, 2001).

Numerical models of the fractional crystallization process are broadly consistent with the observed trends. There are, however, several features that remain poorly understood.

### 1.12.5.1 Imperfect Mixing during Crystallization

The compositional data scatter from the average trend for each group are significantly greater than the analytical uncertainty, in particular for compatible elements (Pernicka and Wasson, 1987; Haack and Scott, 1992, 1993; Scott *et al.*, 1996; Wasson, 1999; Wasson and Richardson, 2001). The scatter shows that the assumption of metal crystallizing from a perfectly mixed liquid breaks down during the course of crystallization. An interesting example of this scatter is observed among and within the multiton fragments of the IIIAB iron meteorite Cape York (Esbensen and Buchwald, 1982; Esbensen *et al.*, 1982). The compositional trend defined by the different Cape York fragments diverges from the general trend defined by IIIAB iron meteorites (Figure 6). The observation that the compositional variation within a single meteorite shower covers most of the scatter within the entire group suggests that the compositional scatter of group IIIAB is due to processes operating on a meter scale. Wasson (1999) noted that both the Cape York trends and the scatter in the IIIAB compositions tend to fall between the compositions of solid metal and its inferred coexisting liquid. Using modified distribution coefficients, he was able to model the Cape York trend as a mixing line between liquid and solid (Figure 6). He suggested that the observed scatter and the Cape York trend are caused by diffusional homogenization of trapped melt pools and solid metal.

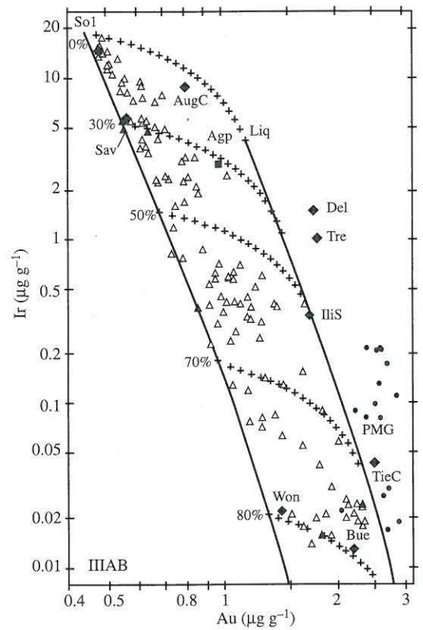


**Figure 6** Solid (left) and liquid (right) tracks shown on a plot of Ir versus Au. Crosses at 0%, 30%, 50%, 70%, and 80% crystallization show solid–liquid mixing curves. The compositions of the Cape York irons Savik and Agpalilik fall close to the mixing line calculated for 30% crystallization. Also shown are the unusual IIIAB meteorites Augusta County, Buenaventura, Delegate, Ilinskaya Stanitza, Tieraco Creek, Treysa, and Wonyulgunna (source Wasson, 1999).

### 1.12.5.2 Late-stage Crystallization and Immiscible Liquid

For most groups the modeled compositional trends tend to deviate from the observations toward the late stages of the crystallization (Figure 5). There are several possible reasons for these discrepancies. The distribution coefficients are functions of the concentration of the incompatible elements sulfur and phosphorus in the liquid. The phosphorus concentration of the melt is well constrained but the behavior of sulfur during crystallization remains poorly understood. Sulfur is almost insoluble in solid metal, and it is therefore not possible to estimate the liquid concentration by analyzing iron meteorites that represent the crystallized metal. Sulfur may only be determined indirectly by treating it as a free parameter in the fractional crystallization models and choose the sulfur composition that provides the best fit to the data (Jones and Drake, 1983; Haack and Scott, 1993; Chabot and Drake, 2000). The concentration of sulfur in the liquid as crystallization proceeds would lead to changes in the slope of the elemental trends that are not matched by observations. Apparently, the distribution coefficients are either incorrect (Wasson, 1999) or some mechanism prevented the concentration of sulfur in the late-stage liquid (Haack and Scott, 1993; Chabot and Drake, 1999).

As sulfur and phosphorus concentrations increase, liquid immiscibility may also play an increasingly important role. Experiments show that at high sulfur and phosphorus concentrations (and high oxygen fugacity), the liquid will enter a two-phase field (Jones and Drake, 1983; Chabot and Drake, 2000) (Figure 7). Ulff-Møller (1998)

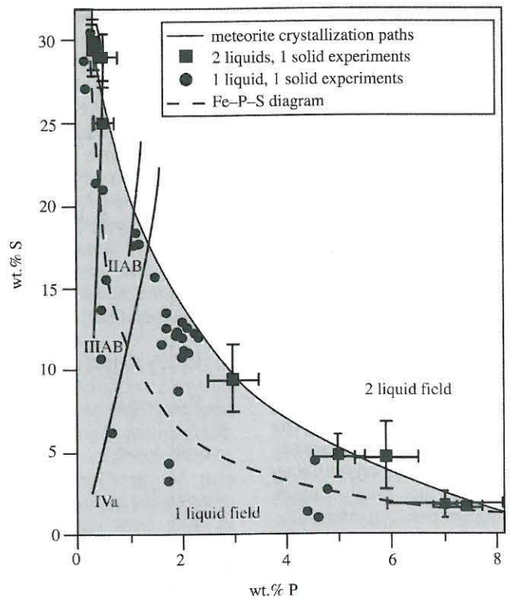


**Figure 7** Two-liquid field in the Fe–S–P system as determined by Raghavan (1988) (hatched line) and Chabot and Drake (2000) (white area). Chabot and Drake performed their experiment at more oxidizing condition—assumed relevant for group IIIAB iron meteorites. Also shown are the trends followed by the major iron meteorite groups. Note that all groups eventually enter the two-liquid field (reproduced by permission of the Meteoritical Society from *Meteorit. Planet. Sci.*, **2000**, *35*, 807–816).

modeled the crystallization of the IIIAB core taking liquid immiscibility into account. He found that the effect of liquid immiscibility changes the compositional trends resulting from late-stage crystallization significantly.

#### 1.12.5.3 The Missing Sulfur-rich Meteorites

Models predict that a considerable volume of Fe,Ni–FeS eutectic melt should be produced at the end of core crystallization. However, the number of sulfur-rich meteorites falls far short of the predicted abundances. For the sulfur- and phosphorus-rich group IIAB, the models predict that the unsampled volume of eutectic melt is ~70% (Chabot and Drake, 2000). Although arguments may be made that the sulfur-rich material is weaker and, therefore, more easily broken down in space and ablates more rapidly during atmospheric entry (Kracher and Wasson, 1982), it remains a mystery why the number of sulfur-rich meteorites is so low. It is, however, worth noting that although the mantle and crust probably comprised more than 85 vol.% of differentiated parent bodies, achondrites that could represent mantle and crust materials of the iron meteorite parent bodies are astonishingly rare. Clearly, processes that selectively remove more fragile materials en route to the Earth are of significant importance.

### 1.12.6 COOLING RATES AND SIZES OF PARENT BODIES

After the cores of the differentiated asteroids had crystallized, a slow cooling period commenced. During this period the most prominent feature of iron meteorites evolved—the Widmanstätten pattern (Figure 8). Several characteristics of the Widmanstätten pattern may be used to constrain the thermal evolution and the sizes of the iron meteorite parent bodies.

In a typical parent-body core with nickel concentrations in the range 7–15 wt.% Ni, the low-nickel phase kamacite will grow at the expense of the high-nickel phase taenite between 800 °C and 500 °C. Several other elements are partitioned between the two phases during growth of the kamacite phase (Rasmussen *et al.*, 1988). The kamacite grows as platelets in four possible orientations relative to the taenite host. Since most



**Figure 8** Widmanstätten pattern in a polished and etched section of the IID iron meteorite, Carbo. 10 cm field of view. The brownish tear shaped troilite nodule to the left has acted as precipitation site for kamacite (Geological Museum, University of Copenhagen, specimen 1990.143).

parent taenite crystals had dimensions larger than typical meteorites, a continuous pattern of four different sets of kamacite plates may be observed on etched surfaces of typical iron meteorites. The limiting factor for the growth of kamacite is the slow diffusion of nickel through taenite. Nickel profiles across taenite lamellae may, therefore, be used to determine the so-called metallographic cooling rate of the parent-body core at ~500 °C (Wood, 1964; Rasmussen, 1981; Herpfer *et al.*, 1994; Yang *et al.*, 1997; Hopfe and Goldstein, 2001; Rasmussen *et al.*, 2001). A number of revisions of the metallographic cooling rate method have been implemented since its original formulation (Wood, 1964; Goldstein and Ogilvie, 1965). Revisions have resulted from improved ternary (Fe–Ni–P) phase diagrams (Doan and Goldstein, 1970; Romig and Goldstein, 1980; Yang *et al.*, 1996) and, in particular, the discovery that small amounts of phosphorus may increase the diffusion rate of nickel through taenite by an order of magnitude (Narayan and Goldstein, 1985; Dean and Goldstein, 1986).

Several other characteristics of the Widmanstätten pattern have provided additional information on the thermal history of the metal. Diffusion controlled growth of schreibersite has been used to determine cooling rates of hexahedrites (Randich and Goldstein, 1978). Although nickel diffusion through kamacite is much faster than through taenite, the decreasing temperature will eventually result in zoned kamacite as well. Zoned kamacite has been used to infer cooling rates at temperatures below 400 °C (Haack *et al.*, 1996b; Rasmussen *et al.*, 2001). Yang *et al.* (1997) showed that the size of the so-called island phase is inversely correlated with cooling rate and may be used to infer the cooling rate at temperatures ~320 °C. The island phase is high-nickel tetrataenite that forms irregular globules with dimensions up to 470 nm in the nickel-rich rims of taenite.

With the exception of group IVA iron meteorites, the metallographic cooling rates tend to be similar within each group but different from group to group (Table 2). This is consistent with the idea that each iron meteorite group cooled in its own separate metallic core surrounded by an insulating mantle. The cooling rates for the different groups of iron meteorites are generally in the range 10–100 °C $Myr^{-1}$.

The metallographic cooling rates combined with numerical models of the thermal evolution of the parent bodies may be used to constrain the sizes of the parent bodies (Wood, 1964; Goldstein and Short, 1967; Haack *et al.*, 1990). The main uncertainties in the numerical models are the states of the mantle, surface, and crust during cooling. Observations of present-day asteroids show that they tend to be covered by a thick insulting regolith and that they may be heavily brecciated. A brecciated mantle and/or a highly porous regolith cover on the surface of an asteroid could potentially slow the cooling rate by a factor of 5–10 (Haack *et al.*, 1990). An approximate relationship between metallographic cooling rates and parent-body radius for regolith covered asteroids was given by Haack *et al.* (1990): $R = 149 \times CR^{-0.465}$, where $R$ is the radius in km and CR the cooling rate in K $Myr^{-1}$. Table 2 gives a compilation of cooling rates and corresponding parent-body sizes.

**Table 2** Metallographic cooling rates and corresponding parent-body radii of the main iron and stony-iron meteorite groups.

| *Group* | *Cooling rate* (K $Myr^{-1}$) | *Parent-body radius* (km) | *Refs.* |
|---|---|---|---|
| IAB | 25 | >33 | a |
| IIAB | 6–12 | 45–65 | b |
| IIIAB | 15–85 | 20–40 | c |
| | 7.5–15 | 42–58 | a |
| IVA | 19–3,400 | >40 | d |
| IVB | 170–230 | 12–14 | e |
| Pallasites | 2.5–4 | 80–100 | a |
| Mesosiderites | 0.5 | 200 | a |

References: (a) Yang *et al.* (1997), (b) Saikumar and Goldstein (1988), (c) Rasmussen (1989), (d) Rasmussen *et al.* (1995), and (e) Rasmussen *et al.* (1984). A radius of the parent body can only be calculated for those groups where the meteorites are believed to have cooled in the core. For other groups a minimum parent-body size may be calculated.

### 1.12.7 PALLASITES

Pallasites are the most abundant group of stony-irons. Their features are easily reconciled with simple models of asteroid differentiation, yet challenge some of our basic assumptions about core formation and crystallization (Mittlefehldt *et al.*, 1998). The 50 known pallasites are divided into main group pallasites, the Eagle Station grouplet (three members) and the pyroxene pallasite grouplet (two members). These are distinguished based on oxygen isotopic, mineral, and metal compositions. Main group pallasites are comprised of subequal mixtures of forsteritic olivine and iron, nickel metal, often heterogeneously distributed. Clusters of olivine grains reach several centimeters (Ulff-Møller *et al.*, 1998), while Brenham has metal cross-cutting zones with more typical pallasitic texture (Figure 9). Olivine morphology also differs significantly, from angular–subangular in Salta to rounded in Thiel mountains (Buseck, 1977; Scott, 1977b).

Olivines in the main group pallasites cluster around $Fo_{88\pm1}$, although some reach $Fo_{82}$, and exhibit core-to-rim zoning of aluminum, chromium, calcium, and manganese (Zhou and Steele, 1993; Hsu *et al.*, 1997). Chromite, low-calcium pyroxene and a variety of phosphates comprise <1 vol.% each (Buseck, 1977; Ulff-Møller *et al.*, 1998). Phosphates show REE patterns, inherited from the olivines, largely consistent with the olivines forming as cumulates at the base of the mantle (Davis and Olsen, 1991; Davis and Olsen, 1996). The metal composition is similar to high-nickel IIIAB irons, but with a greater scatter in nickel (~7–13 wt.%) and some other siderophile elements (Davis, 1977; Scott, 1977b). The pallasite-IIIAB iron link is supported by the similarity in oxygen isotopic compositions of their silicates (Clayton and Mayeda, 1996).

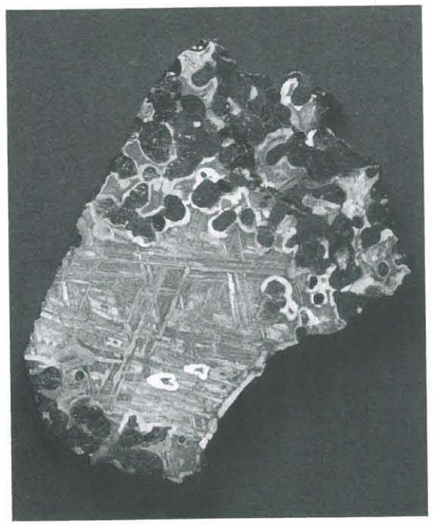

**Figure 9** The Brenham pallasite contains areas of both olivine-free regions and areas more typical of pallasites. In this specimen, pallasitic material is cross-cut by a metallic region, suggesting that silicate–metal mixing at the core–mantle boundary was a dynamic process. Length of specimen is ~13 cm (Smithsonian specimen USNM 266).

The Eagle Station trio (Eagle Station, Cold Bay, Itzawisis) is comprised dominantly of iron and nickel metal and olivine with lesser amounts of clinopyroxene, orthopyroxene, chromite, and phosphates. Olivines in the Eagle Station ($Fo_{80-81}$) are more ferroan than in the main group and differ substantially in their Fe/Mn ratio (Mittlefehldt *et al.*, 1998). Metal in the Eagle Station pallasites has higher iridium and nickel compared to main group pallasites and is closer to metal in IIF irons (Kracher *et al.*, 1980). They also differ dramatically in oxygen isotopic composition from main group pallasites (Clayton and Mayeda, 1996).

Pyroxene pallasites are represented by only two members: Vermillion and Yamato 8451. The two meteorites share the common feature of containing pyroxene, but differ substantially from one another. Yamato 8451 consists of ~60% olivine, 35% metal, 2% pyroxene, and 1% troilite (Hiroi *et al.*, 1993; Yanai and Kojima, 1995). In contrast, Vermillion contains around 14% olivine, and less than 1% each of orthopyroxene, chromite, and phosphates (Boesenberg *et al.*, 2000). The iron concentration in olivine ($Fo_{88-90}$) is similar to main group pallasites, although pyroxene pallasites have lower Fe/Mn ratios (Mittlefehldt *et al.*, 1998). The two pyroxene pallasites do not share a common metal composition with each other or, in detail, with other pallasites (Wasson *et al.*, 1998).

Pallasites are both intriguing and perplexing. The two lithologies, Fe,Ni metal and olivine, are reasonable assemblages expected at the core–mantle boundary of a differentiated asteroid. The lower mantle should be primarily olivine, either a residue from high degrees of partial melting or an early cumulate phase from a global magma ocean. However, the marked density contrast between metal and silicates should lead to rapid separation. Further, some features of pallasitic olivine, such as the angular shapes and marked minor element zoning, seem inconsistent with formation at a relatively quiescent, deep-seated core–mantle boundary. As Mittlefehldt *et al.* (1998) note, the core–mantle boundary origin remains the most plausible, despite these difficulties.

If we assume a core–mantle boundary origin (see Mittlefehldt *et al.*, 1998, for references suggesting alternative models), how can these disparate features be reconciled and what are the implications for the nature of asteroidal cores during cooling and solidification. Scott (1977c) suggested that the main group pallasite metal is a reasonable crystallization product after ~80% crystallization of IIIAB metallic melt. However, asteroidal cores probably crystallized from the core–mantle boundary inwards and we should expect pallasites to have the signature of early-crystallizing, low-nickel melts, not late-crystallizing, high-nickel melts. Haack and Scott (1993) postulated that residual metallic melt migrated to the core–mantle boundary between dendrites and Ulff-Møller *et al.* (1997) proposed mixing of late-stage metallic melt with earlier solidified metal to produce the range of pallasite compositions. Late-stage intrusions might explain the presence of angular olivines, which were fractured during the intrusion (Scott, 1977b), and the heterogeneous textures seen in pallasites like Brenham. Ulff-Møller *et al.* (1997) suggested that high-pressure injection of metal, perhaps caused by impact, might provide the most plausible mechanism for producing pallasites. Finally, pallasites have experienced a long history of subsolidus cooling and annealing. Both minor-element zoning in olivine and rounded olivines might be best explained by subsolidus annealing and diffusion. The small Eagle Station and pyroxene-bearing pallasite grouplets remain enigmatic, but suggest that similar processes operated on other parent bodies and may have been common among highly differentiated asteroids.



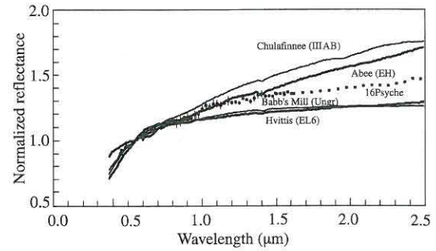


**Figure 10** Normalized reflectance versus wavelength (μm) for M-type 16 Psyche versus iron and enstatite chondrite meteorites (lines) (Gaffey, 1976; Bell *et al.*, 1988; Bus, 1999). All spectra are normalized to unity at 0.55 μm. Spectra for all three are relatively featureless with red spectral slopes and moderate albedos. While some M-class asteroids may be metallic core material, existing spectral and density data are inconsistent with this explanation for all M asteroids.

### 1.12.8 PARENT BODIES OF IRON AND STONY-IRON METEORITES

While iron and stony-iron meteorites provide important snapshots of the origin and evolution of highly differentiated asteroids, they lack geologic context. From which type of asteroid do iron and stony-iron meteorites originate? Are there enough metallic asteroids to account for the enormous diversity among iron meteorites, particularly the ungrouped irons? Have we sampled corresponding abundances of crustal and mantle material in both the meteorite and asteroid populations? These are the questions that we explore in this section.

The major tool that allows us to relate classes of meteorites to classes of asteroids is spectral reflectance (Burbine *et al.*, 2002). Unfortunately, iron meteorites, with their paucity of silicate phases, have relatively featureless spectra with red spectral slopes and moderate albedos (e.g., Cloutis *et al.*, 1990) (Figure 10). There appears to be no simple correlation between nickel abundance and spectra redness and, thus, distinguishing different chemical groups (e.g., low-nickel IIAB from high-nickel IVB) is probably not possible. Historically, M-class asteroids, of which ~40 are known (Tholen, 1989), have been linked to iron meteorites. These asteroids exhibit moderate visual albedos, relatively featureless spectra and red spectral slopes, similar to that of iron meteorites. Radar albedos—an indirect measure of near-surface bulk density—have been used as supporting evidence for the link between iron meteorites and M-class asteroids, as M asteroids tend to have higher radar albedos than C or S asteroids (Magri *et al.*, 1999) and the highest asteroid radar albedos are known from the M asteroids 6178 (1986 DA) and 216 Kleopatra (Ostro *et al.*, 1991, 2000). There is reason to believe that not all (perhaps not many) M-class asteroids are either core fragments or largely intact stripped cores of differentiated asteroids. The enstatite chondrites also exhibit nearly featureless spectra (owing to the nearly $Fe^{2+}$-free composition of the enstatite; Keil, 1968) with red spectral slopes and moderate albedos (Gaffey, 1976) and have been suggested as possible meteoritic analogues to M asteroids (Gaffey and McCord, 1978) (Figure 10). Rivkin *et al.* (2000) found that more than one-third of observed M-class asteroids have 3 μm absorption features suggestive of hydrated silicates. Although this conclusion remains the subject of significant debate (Gaffey *et al.*, 2002a; Rivkin *et al.*, 2002), it would be inconsistent with core material. Finally, recent ground-based measurements of bulk densities for M asteroids 16 Psyche (Viateau, 2000; Britt *et al.*, 2002) and 22 Kalliope (Margot and Brown, 2001) are ~2 g $cm^{-3}$, far below that expected for even highly fragmented core material.

Equally puzzling is the lack of olivine-rich asteroids corresponding to the large numbers of

asteroidal cores sampled by iron meteorites. If we have sampled ~65 asteroidal cores, we might expect corresponding abundances of olivine-rich meteorites and A-type (olivine-rich) asteroids (Chapman, 1986; Bell *et al.*, 1989; Burbine *et al.*, 1996; Gaffey *et al.*, 2002b). The near absence of dunite meteorites and paucity of A-type asteroids has come to be known as "The Great Dunite Shortage." The most likely explanation centers on the age of disruption of differentiated parent bodies and the durability of metallic meteorites and asteroids relative to their stony counterparts. If disruption of differentiated bodies occurred relatively early in the history of the solar system, the dunitic mantle may have been fragmented to below the current observational limit of ~5 km. Dunitic meteorites may well have fallen to Earth as a consequence of this fragmentation of the mantles, but terrestrial ages for meteorites stretch back only ~2 Myr (Welten *et al.*, 1997). In contrast, core fragments may prove much more versatile and may still be sampled by impacts today. Indeed, iron meteorites are much more durable, with cosmic-ray exposure ages to more than 2 Gyr (e.g., Deep Springs, Voshage and Feldmann, 1979). Much slower Yarkovsky-driven transfer times from the asteroid belt for metallic objects also suggest that these sample impacts further back in time (Farinella *et al.*, 1998).

## 1.12.9 FUTURE RESEARCH DIRECTIONS

In this chapter, we have touched upon our current state of knowledge about iron and stony-iron meteorites, the processes that formed them and the places from which they originate. Our knowledge of all of these is far from complete. In this section, we briefly address the future of these fields. What questions remain unanswered? Which are most pressing to understand the origin of iron meteorites? What tools do we need to move forward?

As students of meteorites, our first inclination is to look to the meteorite record for missing types and new meteorite recoveries to fill those gaps. The substantial number of ungrouped iron meteorites suggests that the cores of differentiated bodies are poorly sampled. Additional recoveries may serve to establish new groups that include existing ungrouped irons. However, the number of ungrouped irons continues to grow much more rapidly than the number of new groups. A more fundamental recovery that would increase our understanding of the relative roles of late-stage melt trapping versus concentration would be the discovery of a large (several kilograms), sulfide meteorite. As we noted earlier, few meteorites exist that can reasonably be attributed to a eutectic melt in both phase proportions and compositions. A second field ripe for future work is experimental studies designed to increase our understanding of the processes of core crystallization. Although we now have more than a rudimentary understanding of core crystallization, uncertainties in both partition coefficients (particularly as a function of sulfur, phosphorus, and carbon concentration) and liquid immiscibility in sulfur-, phosphorus-, and carbon-rich systems limit our understanding of the nature of late-stage core crystallization. Recent experimental studies have made significant headway in these areas, and parametrization of partitioning data allows firm predictions about partitioning over a much broader range of conditions, but experimental verification and determination are essential to further strengthen our understanding of these processes.

At the dawn of the twenty-first century, spacecraft missions hold the promise of finally placing meteorites in the context of the worlds from which they came. Although, to our knowledge, none are currently proposed, there is considerable reason to contemplate a mission to an iron meteorite parent body. A mission to a metal-dominated asteroid, particularly one that combines multispectral imaging with remote chemical analyses, may reveal the overall structure of the original body and provide answers to some of our long-standing questions. What is the nature of the core–mantle boundary? Are the pallasites typical examples of this boundary? Where is the olivine hiding? What is the structure of exposed metallic cores and what is the distribution of sulfur-rich material?

We already stand at the threshold of a better understanding of asteroids in general and differentiated asteroids in particular. The Galileo and NEAR missions gave us our first closeup looks at the S-class asteroids Gaspra, Ida, and Eros and the C-type asteroid Mathilde. While all are thought to be primitive chondritic bodies, these encounters revealed new insights into the geologic processes that have modified them during 4.5 Ga of impact bombardment. Our knowledge of differentiated asteroids is considerably less clear. The classification system described in Chapter 1.05 divides the meteorites into groups that came from the same parent body or at least from very similar parent bodies. In some cases we may infer the depth relationship between meteorites but we have no information on the horizontal distribution of the samples we have obtained. We cannot tell if they all came from the same fragment of the original asteroid or if they were more uniformly distributed across the parent body. At least some of these questions may be answered by NASA's DAWN mission, which will visit 4 Vesta by the end of the decade. With its complement of multispectral imagers and gamma-ray spectrometer, it should answer many of our questions about the relationship between surficial basaltic materials, deeper-seated (?) pyroxenitic material, and olivine-rich (?) mantle, including their lateral and horizontal relationships.

Asteroid spectroscopy has provided possible links between iron and stony-iron meteorites and their possible parent as discussed in the previous section. Iron meteorites provide evidence that numerous metal objects exist but the lack of spectral features and the surprising low density determined for some M-type asteroids makes it impossible to establish a firm link between iron meteorites and M-type asteroids. The high cosmic-ray exposure ages of iron meteorites show, not surprisingly, that iron–nickel alloys are much more resistant to impacts and space erosion than stony targets. We should, therefore, expect that the surfaces of stripped metal cores or fragments of metal cores display a dramatic cratered terrain unlike anything that we have ever seen before. Although the subtle compositional differences that occur within and between iron meteorite groups could likely not be discerned from orbit, the difference between metal-dominated lithologies, troilite-rich lithologies, and dunitic/pallasitic lithologies could be easily distinguished on the basis of both spectral absorption features (e.g., Britt *et al.*, 1992) and, more readily, orbital X-ray or gamma-ray compositional mapping finally resolving questions about the existence and/or spatial distribution of these important lithologies. The distribution of sulfur-rich pockets, for example, can provide evidence on the core crystallization process (Haack and Scott, 1992) and the fate of the sulfur-rich material missing from our meteorite collections.

Such a mission might also resolve the role and extent of impact in the formation of asteroidal cores. Impact clearly played a role in the formation of both mesosiderites and silicate-bearing IAB–IIICD irons, but whether those impacts were global or local remains an open question. The slow cooling rates of mesosiderites suggest that the parent body was very large, probably several hundred kilometers in radius (Haack *et al.*, 1996b). Since large asteroids are more difficult to destroy, this opens the possibility that the parent body may still exist. Davis *et al.* (1999) suggested that the largest M-type asteroid, 16 Psyche, could be the shattered remains of the mesosiderite parent body. A mission to Phyche may not only reveal the nature of M-type asteroids, it could also possibly provide evidence on one of the biggest impact events documented in our meteorite collections.

Finally, much has been written in recent years about the hazard presented to mankind by asteroid impact (Gehrels, 1994). While considerable effort has been put into understanding possible mitigation schemes, it is important to remember that energy scales linearly with mass. Thus, a metallic asteroid of comparable diameter would release ~2.5 times the energy of a stony asteroid. Further, its physical properties would certainly be quite different from that of a stony asteroid. The aforementioned mission might not only provide substantial insights into the geologic history of asteroids, but also provide essential data for understanding the physical properties (e.g., material distribution, global cracks) that would allow us to ensure the continuation of human history.



## REFERENCES


Ballhaus C. and Ellis D. J. (1996) Mobility of core melts during Earth's accretion. *Earth Planet. Sci. Lett.* **143**, 137–145.

Bell J. F., Davis D. R., Hartmann W. K., and Gaffey M. J. (1989) Asteroids: the big picture. In *Asteroids II* (eds. R. P. Binzel, T. Gehrels, and M. S. Matthews). University Arizona Press, Tucson, pp. 921–945.

Bell J. F., Owensby P. D., Hawke B. R., and Gaffey M. J. (1988) The 52-color asteroid survey: final results and interpretation (abstract). *Lunar Planet. Sci.* **XIX**. The Lunar and Planetary Institute, Houston, pp. 57–58.

Benedix G. K., McCoy T. J., Keil K., and Love S. G. (2000) A petrologic study of the IAB iron meteorites: constraints on the formation of the IAB-winonaite parent body. *Meteorit. Planet. Sci.* **35**, 1127–1141.

Boesenberg J. S., Davis A. M., Prinz M., Weisberg M. K., Clayton R. N., and Mayeda T. K. (2000) The pyroxene pallasites, Vermillion and Yamato 8451: not quite a couple. *Meteorit. Planet. Sci.* **35**, 757–769.

Bogard D. D. and Garrison D. H. (1998) $^{39}Ar$–$^{40}Ar$ ages and thermal history of mesosiderites. *Geochim. Cosmochim. Acta* **62**, 1459–1468.

Bogard D. D., Garrison D. H., Jordan J. L., and Mittlefehldt D. (1990) $^{39}Ar$–$^{40}Ar$ dating of mesosiderites—evidence for major parent body disruption less than 4 Ga ago. *Geochim. Cosmochim. Acta* **54**, 2549–2564.

Bogard D. D., Garrison D. H., and McCoy T. J. (2000) Chronology and Petrology of silicates from IIE iron meteorites: evidence of a complex parent body evolution. *Geochim. Cosmochim. Acta* **64**, 2133–2154.

Britt D. T., Bell J. F., Haack H., and Scott E. R. D. (1992) The reflectance spectrum of troilite and the T-type asteroids. *Meteoritics* **27**, 207.

Britt D. T., Yeomans D., Housen K., and Consolmagno G. (2002) Asteroid density, porosity, and structure. In *Asteroids III* (eds. W. Bottke, A. Cellino, P. Paolicchi, and R. P. Binzel). University of Arizona Press, Tucson, pp. 485–500.

Buchwald V. F. (1975) *Handbook of Iron Meteorites*. University of California Press, Berkeley, 1426pp.

Buchwald V. F. (1984) Phosphate minerals in meteorites and lunar rocks. In *Phosphate Minerals* (eds. J. O. Nriagu and P. B. Moore). Springer, New York, pp. 199–214.

Burbine T. H., Meibom A., and Binzel R. P. (1996) Mantle material in the main belt: battered to bits? *Meteorit. Planet. Sci.* **31**, 607–620.

Burbine T. H., McCoy T. J., Meibom A., Gladman B., and Keil K. (2002) Meteoritic parent bodies: their number and identification. In *Asteroids III* (eds. W. Bottke, A. Cellino, P. Paolicchi, and R. P. Binzel). University of Arizona Press, Tucson, pp. 653–667.

Bus S. J. (1999) Compositional structure in the asteroid belt: results of a spectroscopic survey. PhD Thesis, Massachusetts Institute of Technology, 367p.

Buseck P. R. (1977) Pallasite meteorites—mineralogy, petrology, and geochemistry. *Geochim. Cosmochim. Acta* **41**, 711–740.

Campbell A. J., Humayun M., Meibom A., Krot A. N., and Keil K. (2001) Origin of zoned metal grains in the QUE94411 chondrite. *Geochim. Cosmochim. Acta* **65**, 163–180.

Chabot N. L. and Drake M. J. (1997) An experimental study of silver and palladium partitioning between solid and liquid metal, with applications to iron meteorites. *Meteorit. Planet. Sci.* **32**, 637–645.

Chabot N. L. and Drake M. J. (1999) Crystallization of magmatic iron meteorites: the role of mixing in the molten core. *Meteorit. Planet. Sci.* **34**, 235–246.

Chabot N. L. and Drake M. J. (2000) Crystallization of magmatic iron meteorites: the effects of phosphorus and liquid immiscibility. *Meteorit. Planet. Sci.* **35**, 807–816.

Chabot N. L. and Jones J. H. (2003) The parameterization of solid metal-liquid metal partitioning of siderophile elements. *Lunar Planet. Sci.* **XXXIV**, #1004. The Lunar and Planetary Institute, Houston (CD-ROM).

Chapman C. R. (1986) Implications of the inferred compositions of the asteroids for their collisional evolution. *Mem. Soc. Astron. Italiana* **57**, 103–114.

Chladni E. F. F. (1794) *Über den Ursprung der von Pallas Gefundenen und anderer ihr ähnlicher Eisenmassen, und Über Einige Damit in Verbindung stehende Naturerscheinungen*. Johan Friedrich Hartknoch, Riga, Latvia, 63p.

Choi B. G., Ouyang X. W., and Wasson J. T. (1995) Classification and origin of IAB and IIICD iron meteorites. *Geochim. Cosmochim. Acta* **59**, 593–612.

Clayton R. N. and Mayeda T. K. (1996) Oxygen isotope studies of achondrites. *Geochim. Cosmochim. Acta* **60**, 1999–2017.

Cloutis E. A., Gaffey M. J., Smith D. G. W., and Lambert R. S. J. (1990) Reflectance spectra of "featureless" materials and the surface mineralogies of M- and E-class asteroid. *J. Geophys. Res.* **95**, 281–293.

Davis A. M. (1977) The cosmochemical history of the pallasites. PhD Dissertation, Yale University, 285p.

Davis A. M. and Olsen E. J. (1991) Phosphates in pallasite meteorites as probes of mantle processes in small planetary bodies. *Nature* **353**, 637–640.

Davis A. M. and Olsen E. J. (1996) REE patterns in pallasite phosphates—a window on mantle differentiation in parent bodies. *Meteorit. Planet. Sci.* **31**, A34.

Davis D. R., Farinella P., and Marzari F. (1999) The missing Psyche family: collisionally eroded or never formed? *Icarus* **137**, 140–151.

Dean D. C. and Goldstein J. I. (1986) Determination of the interdiffusion coefficients in the Fe–Ni and Fe–Ni–P systems below 900 °C. *Metall. Trans.* **17A**, 1131–1138.

Doan A. S. and Goldstein J. I. (1970) The ternary phase diagram Fe–Ni–P. *Metall. Trans.* **1**, 1759–1767.

Esbensen K. H. and Buchwald V. F. (1982) Planet(oid) core crystallization and fractionation: evidence from the Cape York iron meteorite shower. *Phys. Earth Planet. Int.* **29**, 218–232.

Esbensen K. H., Buchwald V. F., Malvin D. J., and Wasson J. T. (1982) Systematic compositional variations in the Cape York iron meteorites. *Geochim. Cosmochim. Acta* **46**, 1913–1920.

Farinella P., Vokrouhlicky D., and Hartmann W. K. (1998) Meteorite delivery via Yarkovsky orbital drift. *Icarus* **132**, 378–387.

Gaetani G. A. and Grove T. L. (1999) Wetting of mantle olivine by sulfide melt: implications for Re/Os ratios in mantle peridotite and late-stage core formation. *Earth Planet. Sci. Lett.* **169**, 147–163.

Gaffey M. J. (1976) Spectral reflectance characteristics of the meteorite classes. *J. Geophys. Res.* **81**, 905–920.

Gaffey M. J. and McCord T. B. (1978) Asteroid surface materials: mineralogical characterizations from reflectance spectra. *Space Sci. Rev.* **21**, 555–628.

Gaffey M. J., Cloutis E. A., Kelley M. S., and Reed K. L. (2002a) Mineralogy of asteroids. In *Asteroids III* (eds. W. Bottke, A. Cellino, P. Paolicchi, and R. P. Binzel). University of Arizona Press, Tucson, pp. 183–204.

Gaffey M. J., Kelley M. S., and Hardersen P. S. (2002b) Meteoritic and asteroidal constraints on the identification and collisional evolution of asteroid families. *Lunar Planet. Sci.* **XXXIII**, #1506. The Lunar and Planetary Institute, Houston (CD-ROM).

Gehrels T. (1994) *Hazards due to Comets and Asteroids*. Tucson, University of Arizona Press, Tucson.

Goldstein J. I. and Friel J. J. (1978) Fractional crystallization of iron meteorites, an experimental study. *Proc. 9th Lunar Planet. Sci. Conf.* 1423–1435.

Goldstein J. I. and Ogilvie R. E. (1965) The growth of the Widmanstätten pattern in metallic meteorites. *Geochim. Cosmochim. Acta* **29**, 893–920.

Goldstein J. I. and Short J. M. (1967) The iron meteorites, their thermal history and parent bodies. *Geochim. Cosmochim. Acta* **31**, 1733–1770.

Grady M. (2000) *Catalogue of Meteorites*. Cambridge University Press, Cambridge.

Haack H. and Scott E. R. D. (1992) Asteroid core crystallization by inward dendritic growth. *J. Geophys. Res.* **97**, 14727–14734.

Haack H. and Scott E. R. D. (1993) Chemical fractionations in group IIIAB iron meteorites—origin by dendritic crystallization of an asteroidal core. *Geochim. Cosmochim. Acta* **57**, 3457–3472.

Haack H., Rasmussen K. L., and Warren P. H. (1990) Effects of regolith megaregolith insulation on the cooling histories of differentiated asteroids. *J. Geophys. Res.* **95**, 5111–5124.

Haack H., Scott E. R. D., Love S. G., Brearley A. J., and McCoy T. J. (1996a) Thermal histories of IVA stony-iron and iron meteorites: evidence for asteroid fragmentation and reaccretion. *Geochim. Cosmochim. Acta* **60**, 3103–3113.

Haack H., Scott E. R. D., and Rasmussen K. L. (1996b) Thermal and shock history of mesosiderites and their large parent asteroid. *Geochim. Cosmochim. Acta* **60**, 2609–2619.

Hassanzadeh J., Rubin A. E., and Wasson J. T. (1989) Large metal nodules in mesosiderites. *Meteoritics* **24** 276–276.

Herpfer M. A. and Larimer J. W. (1993) Core formation: an experimental study of metallic melt-silicate segregation. *Meteoritics* **28**, 362.

Herpfer M. A., Larimer J. W., and Goldstein J. I. (1994) A comparison of metallographic cooling rate methods used in meteorites. *Geochim. Cosmochim. Acta* **58**, 1353–1365.

Hewins R. H. (1983) Impact versus internal origins for mesosiderites. *J. Geophys. Res.* **88**, B257–B266.

Hiroi T., Bell J. F., Takeda H., and Pieters C. M. (1993) Spectral comparison between olivine-rich asteorids and pallasites. *Proc. NIPR Symp. Antarct. Meteorit.* **6**, 234–245.

Hoashi M., Brooks R. R., and Reeves R. D. (1990) The ruthenium content of iron meteorites. *Meteoritics* **25**, 371–372.

Hoashi M., Varelaalvarez H., Brooks R. R., Reeves R. D., Ryan D. E., and Holzbecher J. (1992) Revised classification of some iron meteorites by use of statistical procedures. *Chem. Geol.* **98**, 1–10.

Hoashi M., Brooks R. R., and Reeves R. D. (1993a) Palladium, platinum and ruthenium in iron meteorites and their taxonomic significance. *Chem. Geol.* **106**, 207–218.

Hoashi M., Brooks R. R., Ryan D. E., Holzbecher J., and Reeves R. D. (1993b) Chemical evidence for the pairing of some iron meteorites. *Geochem. J.* **27**, 163–169.

Hopfe W. D. and Goldstein J. I. (2001) The metallographic cooling rate method revised: application to iron meteorites and mesosiderites. *Meteorit. Planet. Sci.* **36**, 135–154.

Horan M. F., Smoliar M. I., and Walker R. J. (1998) $^{182}W$ and $^{187}Re$–$^{187}Os$ systematics of iron meteorites: chronology for melting, differentiation, and crystallization in asteroids. *Geochim. Cosmochim. Acta* **62**, 545–554 (Erratum, 1653).

Hsu W., Huss G. R., and Wasserburg G. J. (1997) Mn–Cr systematics of differentiated meteorites. *Lunar Planet. Sci.* **XXVIII**. The Lunar and Planetary Institute, Houston, pp. 609–610.





Jones J. H. and Drake M. J. (1983) Experimental investigations of trace-element fractionation in iron meteorites: 2, The influence of sulfur. *Geochim. Cosmochim. Acta* **47**, 1199–1209.

Jones J. H. and Malvin D. J. (1990) A nonmetal interaction-model for the segregation of trace-metals during solidification of Fe–Ni–S, Fe–Ni–P, and Fe–Ni–S–P alloys. *Metall. Trans.* **21B**, 697–706.

Keil K. (1968) Mineralogical and chemical relationships among enstatite chondrites. *J. Geophys. Res.* **73**, 6945–6976.

Keil K. (2000) Thermal alteration of asteroids: evidence from meteorites. *Planet. Space Sci.* **48**, 887–903.

Keil K. and Wilson L. (1993) Explosive volcanism and the compositions of cores of differentiated asteroids. *Earth Planet. Sci. Lett.* **117**, 111–124.

Keil K., Haack H., and Scott E. R. D. (1994) Catastrophic fragmentation of asteroids—evidence from meteorites. *Planet. Space Sci.* **42**, 1109–1122.

Keil K., Stöffler D., Love S. G., and Scott E. R. D. (1997) Constraints on the role of impact heating and melting in asteroids. *Meteorit. Planet. Sci.* **32**, 349–363.

Kelly W. R. and Larimer J. W. (1977) Chemical fractionations in meteorites: VIII. Iron meteorites and the cosmochemical history of the metal phase. *Geochim. Cosmochim. Acta* **41**, 93–111.

Kerridge J. F. (1985) Carbon, hydrogen and nitrogen in carbonaceous chondrites abundances and isotopic compositions in bulk samples. *Geochim. Cosmochim. Acta* **49**, 1707–1714.

Kong P. and Ebihara M. (1997) The origin and nebular history of the metal phase of ordinary chondrites. *Geochim. Cosmochim. Acta* **61**, 2317–2329.

Kong P., Mori T., and Ebihara M. (1997) Compositional continuity of enstatite chondrites and implications for heterogeneous accretion of the enstatite chondrite parent body. *Geochim. Cosmochim. Acta* **61**, 4895–4914.

Kracher A. (1985) The evolution of partially differentiated planetesimals: evidence from iron meteorite groups IAB and IIICD. *J. Geophys. Res.* **90**, C689–C698.

Kracher A. and Wasson J. T. (1982) The role of S in the evolution of the parental cores of the iron meteorites. *Geochim. Cosmochim. Acta* **46**, 2419–2426.

Kracher A., Kurat G., and Buchwald V. F. (1977) Cape York: the extraordinary mineralogy of an ordinary iron meteorite and its implication for the genesis of IIIAB irons. *Geochem. J.* **11**, 207–217.

Kracher A., Willis J., and Wasson J. T. (1980) Chemical classification of iron meteorites: IX. A new group (IIF), revision of IAB and IIICD, and data on 57 additional irons. *Geochim. Cosmochim. Acta* **44**, 773–787.

Kullerud G. (1963) The Fe–Ni–S system. *Ann. Rep. Geophys. Lab.* **67**, 4055–4061.

Liu M. H. and Fleet M. E. (2001) Partitioning of siderophile elements (W, Mo, As, Ag, Ge, Ga, and Sn) and Si in the Fe–S system and their fractionation in iron meteorites. *Geochim. Cosmochim. Acta* **65**, 671–682.

Magri C., Ostro S. J., Rosema K. D., Thomas M. L., Mitchell D. L., Campbell D. B., Chandler J. F., Shapiro I. I., Giorgini J. D., and Yeomans D. K. (1999) Mainbelt asteroids: results of Arecibo and Goldstone radar observations of 37 objects during 1980–1985. *Icarus* **140**, 379–407.

Malvin D. J. (1988) Assimilation-fractional crystallization of magmatic iron meteorites. *Lunar Planet. Sci.* **XIX**. Lunar and Planetary Institute, Houston, pp. 720–721.

Malvin D. J., Wang D., and Wasson J. T. (1984) Chemical classification of iron meteorites: X. Multielement studies of 43 irons, resolution of group-IIIE from group-IIIAB and evaluation of Cu as a taxonomic parameter. *Geochim. Cosmochim. Acta* **48**, 785–804.

Malvin D. J., Jones J. H., and Drake M. J. (1986) Experimental investigations of trace-element fractionation in iron meteorites: 3. Elemental partitioning in the system Fe–Ni–S–P. *Geochim. Cosmochim. Acta* **50**, 1221–1231.

Margot J. L. and Brown M. E. (2001) Discovery and characterization of binary asteroids 22 Kalliope and 87 Sylvia. *Bull. Am. Astron. Soc.* **33**, 1133.

McCoy T. J., Keil K., Scott E. R. D., and Haack H. (1993) Genesis of the IIICD iron meteorites: evidence from silicate-bearing inclusions. *Meteoritics* **28**, 552–560.

McCoy T. J., Keil K., Clayton R. N., Mayeda T. K., Bogard D. D., Garrison D. H., Huss G. R., Hutcheon I. D., and Wieler R. (1996) A petrologic, chemical, and isotopic study of monument draw and comparison with other acapulcoites: evidence for formation by incipient partial melting. *Geochim. Cosmochim. Acta* **60**, 2681–2708.

McCoy T. J., Keil K., Clayton R. N., Mayeda T. K., Bogard D. D., Garrison D. H., and Wieler R. (1997a) A petrologic and isotopic study of lodranites: evidence for early formation as partial melt residues from heterogeneous precursors. *Geochim. Cosmochim. Acta* **61**, 623–637.

McCoy T. J., Keil K., Muenow D. W., and Wilson L. (1997b) Partial melting and melt migration in the acapulcoite-lodranite parent body. *Geochim. Cosmochim. Acta* **61**, 639–650.

McCoy T. J., Dickinson T. L., and Lofgren G. E. (1998) Partial melting of the Indarch (EH4) meteorite: textural view of melting and melt migration. *Meteorit. Planet. Sci.* **33**, A100–A101.

Meibom A. and Clark B. E. (1999) Evidence for the insignificance of ordinary chondritic material in the asteroid belt. *Meteorit. Planet. Sci.* **34**, 7–24.

Meibom A., Desch S. J., Krot A. N., Cuzzi J. N., Petaev M. I., Wilson L., and Keil K. (2000) Large-scale thermal events in the solar nebula: evidence from Fe, Ni metal grains in primitive meteorites. *Science* **288**, 839–841.

Minarik W. G., Ryerson F. J., and Watson E. B. (1996) Textural entrapment of core-forming melts. *Science* **272**, 530–533.

Mittlefehldt D. W., Lindstrom M. M., Bogard D. D., Garrison D. H., and Field S. W. (1996) Acapulco- and Lodran-like achondrites: petrology, geochemistry, chronology, and origin. *Geochim. Cosmochim. Acta* **60**, 867–882.

Mittlefehldt D. W., McCoy T. J., Goodrich C. A., and Kracher A. (1998) Non-chondritic meteorites from asteroidal bodies. *Rev. Min.* **36**, D1–D195.

Moore C. B., Lewis C. F., and Nava D. (1969) Superior analysis of iron meteorites. In *Meteorite Research* (ed. P. M. Millman). Reidel, Dordrecht, pp. 738–748.

Moren A. E. and Goldstein J. I. (1978) Cooling rate variations of group-IVA iron meteorites. *Earth Planet. Sci. Lett.* **40**, 151–161.

Moren A. E. and Goldstein J. I. (1979) Cooling rates of group IVA iron meteorites determined from a ternary Fe–Ni–P model. *Earth Planet. Sci. Lett.* **43**, 182–196.

Mostefaoui S., Lugmair G. W., Hoppe P., and El Goresy A. (2003) Evidence for live iron-60 in Semarkona and Chervony Kut: a NanoSIMS atudy. *Lunar Planet. Sci. Conf.* **XXXIV**, #1585. The Lunar and Planetary Institute, Houston (CD-ROM).

Narayan C. and Goldstein J. I. (1981) Experimental determination of ternary partition-coefficients in Fe–Ni–X alloys. *Metall. Trans.* **12A**, 1883–1890.

Narayan C. and Goldstein J. I. (1982) A dendritic solidification model to explain Ge–Ni variations in iron meteorite chemical groups. *Geochim. Cosmochim. Acta* **46**, 259–268.

Narayan C. and Goldstein J. I. (1985) A major revision of iron meteorite cooling rates—an experimental study of the growth of the Widmanstätten pattern. *Geochim. Cosmochim. Acta* **49**, 397–410.

Nyquist E. L., Reese Y., Wiesmann H., Shih C. Y., and Takeda H. (2001) Dating eucrite formation and metamorphism. In *Antarctic Meteorites XXVI*. National Institute for Polar Research, Tokyo, pp. 113–115.

Olsen E. and Fredriksson K. (1966) Phosphates in iron and pallasite meteorites. *Geochim. Cosmochim. Acta* **30**, 459–470.

Olsen E., Davis A., Clarke R. S., Jr., Schultz L., Weber H. W., Clayton R., Mayeda T., Jarosewich E., Sylvester P., Grossman L., Wang M.-S., Lipschutz M. E., Steele I. M., and Schwade J. (1994) Watson: a new link in the IIE iron chain. *Meteoritics.* **29**, 200–213.

Olsen E. J., Davis A. M., Clayton R. N., Mayeda T. K., Moore C. B., and Steele I. M. (1996) A silicate inclusion in Puente del Zacate, a IIIA iron meteorite. *Science* **273**, 1365–1367.

Olsen E. J., Kracher A., Davis A. M., Steele I. M., Hutcheon I. D., and Bunch T. E. (1999) The phosphates of IIIAB iron meteorites. *Meteorit. Planet. Sci.* **34**, 285–300.

Ostro S. J., Campbell D. B., Chandler J. F., Hine A. A., Hudson R. S., Rosema K. D., and Shapiro I. I. (1991) Asteroid 1986 DA: radar evidence for a metallic composition. *Science* **252**, 1399–1404.

Ostro S. J., Hudson R. S., Nolan M. C., Margot J. L., Scheeres D. J., Campbell D. B., Magri C., Giorgini J. D., and Yeomans D. K. (2000) Radar observations of asteroid 216 Kleopatra. *Science* **288**, 836–839.

Pernicka E. and Wasson J. T. (1987) Ru, Re, Os, Pt and Au in iron meteorites. *Geochim. Cosmochim. Acta* **51**, 1717–1726.

Petaev M. I., Meibom A., Krot A. N., Wood J. A., and Keil K. (2001) The condensation origin of zoned metal grains in Queen Alexandra range 94411: implications for the formation of the Bencubbin-like chondrites. *Meteorit. Planet. Sci.* **36**, 93–106.

Powell B. N. (1969) Petrology and chemistry of mesosiderites: I. Textures and composition of nickel–iron. *Geochim. Cosmochim. Acta* **33**, 789–810.

Powell B. N. (1971) Petrology and chemistry of mesosiderites: 2. Silicate textures and compositions and metal-silicate relationships. *Geochim. Cosmochim. Acta* **35**, 5–34.

Prombo C. A. and Clayton R. N. (1985) A striking nitrogen isotope anomaly in the Bencubbin and Weatherford meteorites. *Science* **230**, 935–937.

Prombo C. A. and Clayton R. N. (1993) Nitrogen isotopic compositions of iron meteorites. *Geochim. Cosmochim. Acta* **57**, 3749–3761.

Raghavan V. (1988) The Fe–P–S system. In *Phase Diagrams of Ternary Iron Alloys*. Indian National Scientific Documentation Centre, Vol. 2, pp. 209–217.

Randich E. and Goldstein J. I. (1978) Cooling rates of seven hexahedrites. *Geochim. Cosmochim. Acta* **42**, 221–234.

Rasmussen K. L. (1981) The cooling rates of iron meteorites—a new approach. *Icarus* **45**, 564–576.

Rasmussen K. L. (1982) Determination of the cooling rates and nucleation histories of 8 group IVA iron meteorites using local bulk Ni and P variation. *Icarus* **52**, 444–453.

Rasmussen K. L. (1989) Cooling rates of IIIAB iron meteorites. *Icarus* **80**, 315–325.

Rasmussen K. L., Malvin D. J., Buchwald V. F., and Wasson J. T. (1984) Compositional trends and cooling rates of group IVB iron meteorites. *Geochim. Cosmochim. Acta* **48**, 805–813.

Rasmussen K. L., Malvin D. J., and Wasson J. T. (1988) Trace-element partitioning between taenite and kamacite—relationship to the cooling rates of iron meteorites. *Meteoritics* **23**, 107–112.

Rasmussen K. L., Ulff-Møller F., and Haack H. (1995) The thermal evolution of IVA iron meteorites—evidence from metallographic cooling rates. *Geochim. Cosmochim. Acta* **59**, 3049–3059.

Rasmussen K. L., Haack H., and Ulff-Møller F. (2001) Metallographic cooling rates of group IIF iron meteorites. *Meteorit. Planet. Sci.* **36**, 883–896.

Reid A. M., Williams R. J., and Takeda H. (1974) Coexisting bronzite and clinobronzite and thermal evolution of the Steinbach meteorite. *Earth Planet. Sci. Lett.* **22**, 67–74.

Rivkin A. S., Howell E. S., Lebofsky L. A., Clark B. E., and Britt D. T. (2000) The nature of M-class asteroids from 3 μm observations. *Icarus* **145**, 351–368.

Rivkin A. S., Howell E. S., Vilas F., and Lebofsky L. A. (2002) Hydrated minerals on asteroids: the astronomical record. In *Asteroids III* (eds. W. Bottke, A. Cellino, P. Paolicchi, and R. P. Binzel). University of Arizona Press, Tucson, pp. 235–253.

Romig A. D. and Goldstein J. I. (1980) Determination of the Fe–Ni and Fe–Ni–P phase diagrams at low temperatures (700 to 300°C). *Metall. Trans. 11A*, 1151–1159.

Rubin A. E. and Mittlefehldt D. W. (1992) Mesosiderites—a chronological and petrologic synthesis. *Meteoritics* **27**, 282–282.

Rushmer T., Minarik W. G., and Taylor G. J. (2000) Physical processes of core formation. In *Origin of the Earth and Moon* (eds. R. M. Canup and K. Righter). University of Arizona Press, Tucson, pp. 227–243.

Ruzicka A., Fowler G. W., Snyder G. A., Prinz M., Papike J. J., and Taylor L. A. (1999) Petrogenesis of silicate inclusions in the weekeroo station IIE iron meteorite: differentiation, remelting, and dynamic mixing. *Geochim. Cosmochim. Acta* **63**, 2123–2143.

Saikumar V. and Goldstein J. I. (1988) An evaluation of the methods to determine the cooling rates of iron meteorites. *Geochim. Cosmochim. Acta* **52**, 715–726.

Schaudy R., Wasson J. T., and Buchwald V. F. (1972) Chemical classification of iron meteorites: VI. Reinvestigation of irons with Ge concentrations lower than 1 ppm. *Icarus* **17**, 174–192.

Scott E. R. D. (1972) Chemical fractionation in iron meteorites and its interpretation. *Geochim. Cosmochim. Acta* **36**, 1205–1236.

Scott E. R. D. (1977a) Composition, mineralogy and origin of group IC iron meteorites. *Earth Planet. Sci. Lett.* **37**, 273–284.

Scott E. R. D. (1977b) Formation of olivine-metal textures in pallasite meteorites. *Geochim. Cosmochim. Acta* **41**, 693–710.

Scott E. R. D. (1977c) Geochemical relationships between some pallasites and iron meteorites. *Min. Mag.* **41**, 265–272.

Scott E. R. D. (1978) Tungsten in iron meteorites. *Earth Planet. Sci. Lett.* **39**, 363–370.

Scott E. R. D. (1979) Origin of anomalous iron meteorites. *Mineral. Mag.* **43**, 415–421.

Scott E. R. D. and Wasson J. T. (1975) Classification and properties of iron meteorites. *Rev. Geophys. Space Phys.* **13**, 527–546.

Scott E. R. D. and Wasson J. T. (1976) Chemical classification of iron meteorites: VIII. Groups IC, IIE, IIIF and 97 other irons. *Geochim. Cosmochim. Acta* **40**, 103–115.

Scott E. R. D., Wasson J. T., and Buchwald V. F. (1973) Chemical classification of iron meteorites: VII. Reinvestigation of irons with Ge concentrations between 25 and 80 ppm. *Geochim. Cosmochim. Acta* **37**, 1957–1983.

Scott E. R. D., Haack H., and McCoy T. J. (1996) Core crystallization and silicate-metal mixing in the parent body of the IVA iron and stony-iron meteorites. *Geochim. Cosmochim. Acta* **60**, 1615–1631.

Scott E. R. D., Haack H., and Love S. G. (2001) Formation of mesosiderites by fragmentation and reaccretion of a large differentiated asteroid. *Meteorit. Planet. Sci.* **36**, 869–881.

Shannon M. C. and Agee C. B. (1996) High pressure constraints on percolative core formation. *Geophys. Res. Lett.* **23**, 2717–2720.

Shannon M. C. and Agee C. B. (1998) Percolation of core melts at lower mantle conditions. *Science* **280**, 1059–1061.

Shukolyukov A. and Lugmair G. (1992) $^{60}$Fe-Light my fire. *Meteoritics* **27**, 289.

Smoliar M. I., Walker R. J., and Morgan J. W. (1996) Re–Os ages of group IIA, IIIA, IVA, and IVB iron meteorites. *Science* **271**, 1099–1102.

Sonett C. P., Colburn D. S., Schwartz K., and Keil K. (1970) The melting of asteroidal-sized parent bodies by unipolar dynamo induction from a primitive T Tauri sun. *Astrophys. Space Sci.* **7**, 446–488.





Srinivasan G., Goswami J. N., and Bhandari N. (1999) $^{26}$Al in eucrite Piplia Kalan: plausible heat source and formation chronology. *Science* **284**, 1348–1350.

Stöffler D., Bischoff A., Buchwald V. F., and Rubin A. E. (1988) Shock effects in meteorites. In *Meteorites and the Early Solar System* (eds. J. F. Kerridge and M. S. Matthews). University of Arizona Press, Tucson, pp. 165–204.

Tachibana S. and Huss G. I. (2003) The initial abundance of $^{60}$Fe in the solar system. *Astrophys. J.* **588**, L41–L44.

Takahashi E. (1983) Melting of a Yamato L3 chondrite (Y-74191) up to 30 kbar. *Proc. 8th Symp. Antarct. Meteorit.*, 168–180.

Taylor G. J. (1992) Core formation in asteroids. *J. Geophys. Res.* **97**, 14717–14726.

Taylor G. J., Keil K., McCoy T., Haack H., and Scott E. R. D. (1993) Asteroid differentiation—pyroclastic volcanism to Magma Oceans. *Meteoritics* **28**, 34–52.

Tholen D. J. (1989) Asteroid taxonomic classification. In *Asteroids II* (eds. R. P. Binzel, T. Gehrels, and M. S. Matthews). University of Arizona Press, Tucson, pp. 1139–1150.

Ulff-Møller F. (1998) Effects of liquid immiscibility on trace element fractionation in magmatic iron meteorites: a case study of group IIIAB. *Meteorit. Planet. Sci.* **33**, 207–220.

Ulff-Møller F., Rasmussen K. L., Prinz M., Palme H., Spettel B., and Kallemeyn G. W. (1995) Magmatic activity on the IVA parent body—evidence from silicate-bearing iron meteorites. *Geochim. Cosmochim. Acta* **59**, 4713–4728.

Ulff-Møller F., Tran J., Choi B.-G., Haag R., Rubin A. E., and Wasson J. T. (1997) Esquel: implications for pallasite formation processes based on the petrography of a large slab. *Lunar Planet. Sci.* **XXVIII**. The Lunar and Planetary Institute, Houston, pp. 1465–1466.

Ulff-Møller F., Choi B. G., Rubin A. E., Tran J., and Wasson J. T. (1998) Paucity of sulfide in a large slab of Esquel: new perspectives on pallasite formation. *Meteorit. Planet. Sci.* **33**, 221–227.

Urakawa S., Kato M., and Kumazawa M. (1987) Experimental study on the phase relations in the system Fe–Ni–O–S up to 15 GPa. In *High Pressure Research in Mineral Physics*. TERRAPUB/AGU, pp. 95–111.

Viateau B. (2000) Mass and density of asteroids (16) psyche and (121) Hermione. *Astron. Astrophys.* **354**, 725–731.

Voshage H. (1967) Bestrahlungsalter und Herkunft der Eisenmeteorite. *Z. Naturforschg.* **22a**, 477–506.

Voshage H. and Feldmann H. (1979) Investigations on cosmic-ray-produced nuclides in iron meteorites: 3. Exposure ages, meteoroid sizes and sample depths determined by mass-spectrometric analyses of Potassium and rare gases. *Earth Planet. Sci. Lett.* **45**, 293–308.

Walker D. and Agee C. B. (1988) Ureilite compaction. *Meteoritics* **23**, 81–91.

Wasson J. T. (1967) Chemical classification of iron meteorites: I. A study of iron meteorites with low concentrations of gallium and germanium. *Geochim. Cosmochim. Acta* **31**, 161–180.

Wasson J. T. (1969) Chemical classification of iron meteorites: III. Hexahedrites and other irons with germanium concentrations between 80 ppm and 200 ppm. *Geochim. Cosmochim. Acta* **33**, 859–876.

Wasson J. T. (1970) Chemical classification of iron meteorites: IV. Irons with Ge concentrations greater than 190 ppm and other meteorites associated with group I. *Icarus* **12**, 407–423.

Wasson J. T. (1971) Chemical classification of iron meteorites: V. Groups IIIC and IIID and other irons with germanium concentrations between 1 and 25 ppm. *Icarus* **14**, 59–70.

Wasson J. T. (1990) Ungrouped iron meteorites in Antarctica—origin of anomalously high abundance. *Science* **249**, 900–902.

Wasson J. T. (1999) Trapped melt in IIIAB irons: solid/liquid elemental partitioning during the fractionation of the IIIAB magma. *Geochim. Cosmochim. Acta* **63**, 2875–2889.

Wasson J. T. and Kallemeyn G. W. (2002) The IAB iron-meteorite complex: a group, five subgroups, numerous grouplets, closely related, mainly formed by crystal segregation in rapidly cooling melts. *Geochim. Cosmochim. Acta* **66**, 2445–2473.

Wasson J. T. and Kimberlin J. (1967) Chemical classification of iron meteorites: II. Irons and pallasites with germanium concentrations between 8 and 100 ppm. *Geochim. Cosmochim. Acta* **31**, 2065–2093.

Wasson J. T. and Richardson J. W. (2001) Fractionation trends among IVA iron meteorites: contrasts with IIIAB trends. *Geochim. Cosmochim. Acta* **65**, 951–970.

Wasson J. T. and Rubin A. E. (1985) Formation of mesosiderites by low-velocity impacts as a natural consequence of planet formation. *Nature* **318**, 168–170.

Wasson J. T. and Wai C. M. (1976) Explanation for the very low Ga and Ge concentrations in some iron meteorite groups. *Nature* **261**, 114–116.

Wasson J. T. and Wang J. M. (1986) A nonmagmatic origin of group IIE iron meteorites. *Geochim. Cosmochim. Acta* **50**, 725–732.

Wasson J. T., Ouyang X. W., Wang J. M., and Jerde E. (1989) Chemical classification of iron meteorites: XI. Multi-element studies of 38 new irons and the high abundance of ungrouped irons from Antarctica. *Geochim. Cosmochim. Acta* **53**, 735–744.

Wasson J. T., Choi B. G., Jerde E. A., and Ulff-Møller F. (1998) Chemical classification of iron meteorites: XII. New members of the magmatic groups. *Geochim. Cosmochim. Acta* **62**, 715–724.

Welten K. C., Alderliesten C., Van der Borg K., Lindner L., Loeken T., and Schultz L. (1997) Lewis Cliff 86360: an Antarctic L-chondrite with a terrestrial age of 2.35 million years. *Meteorit. Planet. Sci.* **32**, 775–780.

Willis J. and Goldstein J. I. (1982) The effects of C, P, and S on trace-element partitioning during solidification in Fe–Ni alloys. *J. Geophys. Res.* **87**, A435–A445.

Willis J. and Wasson J. T. (1978a) Cooling rates of group-IVA iron meteorites. *Earth Planet. Sci. Lett.* **40**, 141–150.

Willis J. and Wasson J. T. (1978b) Core origin for group-IVA iron meteorites—reply. *Earth Planet. Sci. Lett.* **40**, 162–167.

Wood J. A. (1964) Cooling rates and parent planets of several iron meteorites. *Icarus* **3**, 429–459.

Yanai K. and Kojima H. (1995) Yamato-8451: a newly identified pyroxene-bearing pallasite. *Proc. NIPR Symp. Antarct. Meteorit.* **8**, 1–10.

Yang C. W., Williams D. B., and Goldstein J. J. (1996) A revision of the Fe–Ni phase diagram at low temperatures (<400 degrees C). *J. Phase Equil.* **17**, 522–531.

Yang C. W., Williams D. B., and Goldstein J. I. (1997) A new empirical cooling rate indicator for meteorites based on the size of the cloudy zone of the metallic phases. *Meteorit. Planet. Sci.* **32**, 423–429.

Zhou H. and Steele I. M. (1993) Chemical zoning and diffusion of Ca, Al, Mn, and Cr in olivine of springwater pallasite. *Lunar Planet. Sci.* **XXIV**. The Lunar and Planetary Institute, Houston, pp. 1573–1574.




*Treatise on Geochemistry*
ISBN (set): 0-08-043751-6
Volume 1; (ISBN: 0-08-044336-2); pp. 325–345